
Enjoy Your Layer Normalization with the Computational Efficiency of RMSNorm

Yuxin Guo¹ Yihao Yue¹ Yunhao Ni¹ Yizhou Ruan¹ Jie Luo¹ Wenjun Wu^{1,2} Lei Huang^{✉1,2}

Abstract

Layer normalization (LN) is a fundamental component in modern deep learning, but its per-sample centering and scaling introduce non-negligible inference overhead. RMSNorm improves efficiency by removing the centering operation, yet this may discard benefits associated with centering. This paper propose a framework to determine whether an LN in an arbitrary DNN can be replaced by RMSNorm without changing the model function. The key idea is to fold LN’s centering operation into upstream general linear layers by enforcing zero-mean outputs through the column-centered constraint (CCC) and column-based weight centering (CBWC). We extend the analysis to arbitrary DNNs, define such LNs as foldable LNs, and develop a graph-based detection algorithm. Our analysis shows that many LNs in widely used architectures are foldable, enabling exact inference-time conversion and end-to-end acceleration of 2% to 12% without changing model predictions. Experiments across multiple task families further show that, when exact equivalence is partially broken in practical training settings, our method remains competitive with vanilla LN while improving efficiency.

1. Introduction

Normalization techniques are widely used in deep neural networks (DNNs) to stabilize and accelerate training (Huang et al., 2023). As a seminal work, Batch Normalization (BN) (Ioffe & Szegedy, 2015) improves the training stability and the optimization efficiency of DNN by standardizing (centering and scaling) the activations of intermediate DNN layers within a mini-batch of data during training. During

inference, BN uses population statistics calculated in training for normalization, and this operation can be folded into upstream linear layers (Jacob et al., 2018), avoiding additional computational cost. Despite many merits, BN suffers from the train-inference inconsistent problem, leading to significantly degenerate performance in the scenarios of small batch sizes training and domain shifted distributions (Huang et al., 2023).

Layer Normalization (LN) (Ba et al., 2016) addresses BN’s train-inference inconsistency by standardizing the inputs of layers across neurons for each individual sample. It has become a key component of Transformer (Vaswani et al., 2017) and its variants (Dai et al., 2019; Xiong et al., 2020; Dosovitskiy et al., 2021), spreading from the Natural Language Processing (NLP) (Radford et al., 2018; Devlin et al., 2019; Raffel et al., 2020) to Computer Vision (CV) (Dosovitskiy et al., 2021; Carion et al., 2020; Cheng et al., 2022) communities. LN plays a foundational role (Huang et al., 2023) in the evolution of neural architectures and is a standard component in many foundation models (Brown et al., 2020a; Alayrac et al., 2022; Kirillov et al., 2023). However, during inference, unlike BN and other normalization-free counterparts, LN must perform per-sample normalization for each sample which introduces non-negligible additional computational cost.

To alleviate the computational burden of LN, RMSNorm (Zhang & Sennrich, 2019) was proposed as a scaling-only normalization method. According to the experiments in (Zhang & Sennrich, 2019), RMSNorm is reported to reduce the running time of LN by 7%–64% across different models. Owing to its great potential in practice for computational efficiency, RMSNorm has been widely adopted in various architectures (Zhang et al., 2024; Team et al., 2024; Mehta et al., 2024). However, by removing the centering operation, RMSNorm may lose some of the conditioning-related benefits commonly associated with centering in prior work (LeCun et al., 1990; Schraudolph, 1998; Montavon & Müller, 2012; Ba et al., 2016; Huang et al., 2017). This raises the question of how we can retain the theoretical advantages of LN while enjoying the computational cost of RMSNorm with mathematical equivalence.

A previous study (Jiang et al., 2023) showed that LN can be

¹State Key Laboratory of Complex and Critical Software Environment (SKLCCSE), Beihang University, Beijing, China
²Hangzhou International Innovation Institute, Beihang University, Hangzhou, China. Correspondence to: Lei Huang <huanleiAI@buaa.edu.cn>.

reduced to RMSNorm in pre-norm Transformers by removing redundant mean information in the main branch, which arises from preprocessing and residual connections. However, their analysis and resulting modification are restricted to the specific structures of pre-norm Transformers, leaving open the question of whether a more general framework can be developed for arbitrary DNNs.

In this work, we propose a general framework for determining whether an LN layer can be replaced with RMSNorm without changing model predictions at inference time or optimization dynamics during training. We first study the case where LN follows a linear layer. In this setting, we formally characterize when the centering operation of an LN becomes redundant and can therefore be removed. To this end, we introduce the column-centered constraint (CCC) (Def. 3.1) on the immediately preceding linear layer, enforced through column-based weight centering (CBWC) (Def. 3.2), a reparameterization of the weight matrix. We show that the CBWC+RMSNorm scheme is mathematically equivalent to the vanilla model in both inference and training.

We then extend the analysis to general neural networks by introducing the notion of a foldable LN (Def. 4.1) and its associated zero-mean graph (Def. 4.2). These concepts characterize, from a graph perspective, the structural conditions under which the centering operation of LN can be folded into upstream general linear layers, thereby allowing LN to be replaced by RMSNorm. Specifically, an LN is foldable when all leaf nodes in its zero-mean graph correspond to general linear layers or layers that already guarantee zero-mean output, so that the zero-mean property required by LN can be enforced through CBWC on the corresponding upstream layers. This analysis also clarifies practical cases in which the centering operation of some LNs can be removed through auxiliary centering rather than through CBWC.

Finally, we present an algorithm for detecting foldable LNs and identifying the corresponding upstream layers requiring CBWC in arbitrary DNNs. Our analysis shows that most LNs in widely used architectures are foldable, enabling straightforward inference acceleration and yielding end-to-end inference acceleration of 2% to 12%. In addition, experiments across multiple task families show that even when exact folding conditions do not fully hold in practical training settings, CBWC+RMSNorm achieves performance comparable to LN while improving efficiency especially in long-sequence tasks. Our code is available at <https://github.com/BobYue-01/Enjoy-LN>.

2. Notation and Preliminaries

We use $x \in \mathbb{R}$, $\mathbf{x} \in \mathbb{R}^n$, and $\mathbf{X} \in \mathbb{R}^{m \times n}$ to denote a scalar, a vector, and a matrix, respectively, where \mathbb{R} is the set of

real numbers and $m, n \in \mathbb{N}_+$. We use $\mathbf{1}_n$ to denote the n -dimensional all-one column vector.

Neural Network. We model a neural network as a function $f(\mathbf{x}; \boldsymbol{\theta})$, where \mathbf{x} is the input and $\boldsymbol{\theta} \in \Theta$ denotes the set of all learnable parameters, partitioned layer-wise as $\boldsymbol{\theta} = \{\boldsymbol{\theta}^{(k)}\}_{k=1}^L$. For an L -layer MLP, the forward pass consists of alternating linear transformations,¹ normalization, and activation:

$$\mathbf{h}^{(k)} = \mathbf{W}(\boldsymbol{\theta}^{(k)}) \mathbf{x}^{(k-1)}, \quad (1)$$

$$\widehat{\mathbf{h}}^{(k)} = \text{Norm}(\mathbf{h}^{(k)}) \quad (2)$$

$$\mathbf{x}^{(k)} = \phi(\widehat{\mathbf{h}}^{(k)}), \quad k = 1, \dots, L, \quad (3)$$

where $\mathbf{x}^{(0)} = \mathbf{x}$ is the input, and $\mathbf{W}(\boldsymbol{\theta}^{(k)}) \in \mathbb{R}^{m \times n}$ is the weight matrix of layer k .²

Layer Normalization. Layer Normalization (LN) is a fundamental component in modern deep neural networks. Given a layer input vector $\mathbf{h} = [h_1, h_2, \dots, h_n]^\top \in \mathbb{R}^n$, LN normalizes \mathbf{h} across its n elements (neurons) through centering and scaling:³

$$\text{Centering : } \tilde{h}_j = h_j - \mu, \quad j = 1, 2, \dots, n, \quad (4)$$

$$\text{Scaling : } \hat{h}_j = \frac{\tilde{h}_j}{\sqrt{\sigma^2 + \epsilon}}, \quad j = 1, 2, \dots, n, \quad (5)$$

where $\mu = \frac{1}{n} \sum_{j=1}^n h_j$ is the mean of \mathbf{h} and $\sigma^2 = \frac{1}{n} \sum_{j=1}^n \tilde{h}_j^2$ is the second moment of the centered vector $\tilde{\mathbf{h}} = [\tilde{h}_1, \tilde{h}_2, \dots, \tilde{h}_n]^\top$. *Centering* enforces zero mean across elements, and the subsequent *scaling* step ensures unit second moment, corresponding to the normalization retained in RMSNorm.

By definition, RMSNorm is computationally simpler than LN because it removes the centering step. However, although RMSNorm enjoys faster speed, it does not explicitly constrain the sample mean, which can lead to a less stable output range and larger variation in activations across layers (see Section 5.1 and Appendix F for details).

In this paper, we aim to reduce the computational overhead of LN by replacing it with RMSNorm. However, a direct substitution may disrupt training dynamics and degrade performance. In Section 3, we present a mathematically equivalent method for replacing LN with RMSNorm when LN directly follows a linear layer. In Section 4, we extend this analysis to arbitrary DNNs and propose an algorithm for

¹Following deep learning conventions, we do not distinguish between linear and affine transformations. The bias term is omitted here for simplicity; its inclusion is discussed in Appendix A.

²For convenience of notation, we simplify $\boldsymbol{\theta}^{(k)}$ to $\boldsymbol{\theta}_k$ in this paper.

³In practice, LN typically includes a learnable affine transformation after normalization, which is omitted here for simplicity. The term ϵ prevents division by zero.

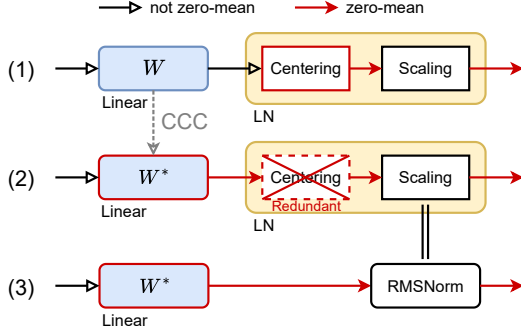


Figure 1. Overview of the method. W denotes the weight matrix of a general linear layer, and W^* is applied with CBWC which satisfies CCC.

automatically detecting and replacing foldable LNs. Finally, in Section 5, we conduct comprehensive experiments to validate the effectiveness and efficiency of the proposed approach.

3. Equivalent Replacement of LN after Linear Layers

In this section, we present a theoretical analysis of the case where LN is applied directly after a linear layer, and show how it can be replaced with RMSNorm in a mathematically equivalent way. We introduce the *column-centered constraint* (CCC), which enforces zero-mean output for the linear layer, as shown in Figure 1. We further propose the *column-based weight centering* (CBWC), a reparameterization that ensures the linear layer satisfies CCC during training. As a result, the CBWC+RMSNorm scheme is mathematically equivalent to the original LN-based model.

3.1. Column-Centered Constraint

We begin with the common case in which LN is applied immediately after a linear layer. Intuitively, the centering step of LN becomes redundant if the output of the linear layer has zero mean across neurons. Since this zero-mean property must hold for all samples, it can be enforced directly through a suitable constraint on the parameters of the linear layer.

We write the linear layer as a linear transformation $\mathbf{h}(\mathbf{x}; \boldsymbol{\theta}_k) = \mathbf{W}(\boldsymbol{\theta}_k) \mathbf{x}$, and denote the columns of $\mathbf{W}(\boldsymbol{\theta}_k)$ by $\mathbf{w}_i(\boldsymbol{\theta}_k) \in \mathbb{R}^m$, i.e., $\mathbf{W}(\boldsymbol{\theta}_k) = [\mathbf{w}_1(\boldsymbol{\theta}_k), \mathbf{w}_2(\boldsymbol{\theta}_k), \dots, \mathbf{w}_n(\boldsymbol{\theta}_k)]$. Under this notation, we define the *column-centered constraint* as follows.

Definition 3.1 (Column-Centered Constraint (CCC)). The parameter $\boldsymbol{\theta}_k \in \Theta^{(k)}$ of a linear layer satisfies the *column-centered constraint* if:

$$\boldsymbol{\theta}_k \in \Theta^* = \{ \boldsymbol{\theta} : \mathbf{w}_i(\boldsymbol{\theta})^\top \mathbf{1}_m = 0, i = 1, 2, \dots, n \} \subseteq \Theta^{(k)}, \quad (6)$$

i.e., the elements in each column vector $\mathbf{w}_i(\boldsymbol{\theta}_k)$ sum to zero.

Proposition 3.1 (Zero-mean Output under CCC). *If the parameters of a linear layer $\boldsymbol{\theta}_k$ satisfy CCC, then for any input $\mathbf{x} \in \mathbb{R}^n$, the output $\mathbf{h} = \mathbf{W}(\boldsymbol{\theta}_k) \mathbf{x}$ has zero mean across its elements, i.e., $\mu_h = \frac{1}{m} \mathbf{1}_m^\top \mathbf{h} = 0$.*

Prop. 3.1 follows directly from Def. 3.1; the full proof is given in Appendix B.1. Therefore, enforcing CCC on the linear layer folds the parameter space $\Theta^{(k)}$ into a subspace Θ^* . Accordingly, the linear layer effectively performs the centering step in advance, making the subsequent use of LN or RMSNorm equivalent.

General Linear Layers. To go beyond standard linear layers, we regard any layer that applies a linear transformation to its input as a general linear layer. Typical examples include recurrent layers with shared weights in RNNs and convolution layers in CNNs. Their parameters can be written in the unified form of Eqn. 1, and the corresponding CCCs are derived in Appendix C.

3.2. Column-Based Weight Centering

To enforce CCC during training, we introduce a reparameterization technique⁴ called *column-based weight centering*, illustrated in Figure 2 and formally defined below.

Definition 3.2 (Column-Based Weight Centering (CBWC)). *Column-based weight centering* introduces a proxy parameter matrix \mathbf{V} by the effective weight matrix \mathbf{W} via the transformation

$$\mathbf{V} = \varphi(\mathbf{W}) = \left(\mathbf{I} - \frac{1}{m} \mathbf{1}_m \mathbf{1}_m^\top \right) \mathbf{W}, \quad (7)$$

where m is the number of output neurons. During back-propagation, the gradient with respect to \mathbf{W} is given by

$$\frac{\partial \mathcal{L}}{\partial \mathbf{W}} = \phi \left(\frac{\partial \mathcal{L}}{\partial \mathbf{V}} \right) = \left(\mathbf{I} - \frac{1}{m} \mathbf{1}_m \mathbf{1}_m^\top \right)^\top \frac{\partial \mathcal{L}}{\partial \mathbf{V}}. \quad (8)$$

Note that CCC can be enforced in many ways. For example, the degenerate subspace $\Theta^* = \{\mathbf{0}\}$ satisfies Eqn. 6, but it destroys the representation capacity of the layer. By contrast, CBWC is a structured reparameterization that enforces CCC while preserving mathematical equivalence with the original model.

Proposition 3.2 (Equivalent Optimization Process). *Consider a model containing a general linear layer followed by LN. Replacing that general linear layer with its CBWC parameterization and replacing LN with RMSNorm yields an optimization process equivalent to that of the original model.*

⁴Reparameterization refers to transforming a model’s parameter space to enforce desired constraints while preserving model capacity (Nowlan et al., 1998).

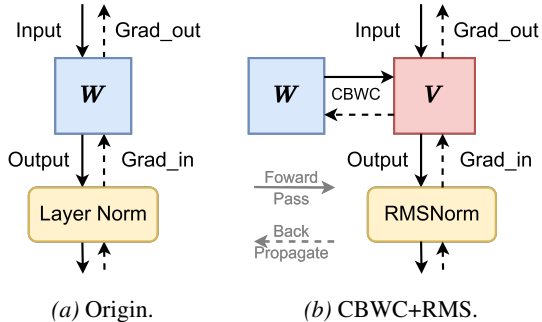


Figure 2. Sketch map of the two training scheme.

The proof of Prop. 3.2 is given in Appendix B.2. Once CBWC is applied to the upstream general linear layer, RMSNorm can replace the LN while producing identical outputs and gradients, yet at lower computational cost. The resulting CBWC+RMSNorm scheme therefore yields parameters that are mathematically equivalent to those of the original LN-based model, which we further discuss in Section 5.4.

Compatibility with Optimization Techniques. From the viewpoint of the optimizer, learning-rate scheduler, gradient clipping, and weight-decay implementation applied on the weight matrix, CBWC+RMSNorm is operationally indistinguishable from the original LN-based model.

Extension to Group Normalization. CCC and CBWC on general linear layers can be extended to Group Normalization (GN) (Wu & He, 2018), which subsumes LN. The resulting grouped-CCC and grouped-CBWC are derived in Appendix C.3.

4. A Framework for Folding LN in Arbitrary DNNs

In this section, we extend the analysis from Section 3 to arbitrary DNNs and develop a general framework for determining whether an LN can be replaced with RMSNorm. We first introduce the notion of a foldable LN and analyze the structural conditions for LN folding in simple but common architectures, including sequential models and models with parallel connections. We then generalize this analysis to arbitrary neural networks from a graph perspective. Finally, we propose an algorithm for automatically detecting foldable LNs and identifying the corresponding upstream general linear layers requiring CBWC.

4.1. Foldable LN in Simple but Common Cases

We begin by studying when an LN in a DNN can be replaced with RMSNorm. Intuitively, an LN is foldable if replacing it with RMSNorm yields identical outputs for all inputs under an appropriate parameter constraint. We formalize this notion as follows.

Definition 4.1 (Foldable LN). Let $f(\cdot; \theta)$ denote a subnetwork that directly precedes an LN layer, and let Θ be the parameter space of this subnetwork. For a non-empty subset $\Theta^* \subseteq \Theta$, we say that this LN is *foldable* with respect to Θ^* if, for all $\theta^* \in \Theta^*$ and all inputs $\mathbf{x} \in \mathbb{R}^n$, it holds that

$$\text{RMSNorm}(f(\mathbf{x}; \theta^*)) = \text{LN}(f(\mathbf{x}; \theta^*)). \quad (9)$$

Although Def. 4.1 is stated for an arbitrary subset $\Theta^* \subseteq \Theta$, in the following analysis we focus on the case where Θ^* is induced by CBWC. This is because Prop. 3.2 establishes the mathematical equivalence between CBWC+RMSNorm and the original LN model in both inference and training. Therefore, restricting Θ^* allows us to keep the analysis concrete.

Extending the analysis from the simple setting in Section 3, whether an LN is foldable is determined by the structure of the model, namely, whether the input to the LN is produced through layers that preserve or enforce the zero-mean property. Therefore, to determine whether an LN is foldable, we backtrack the data flow path and analyze the layers that contribute to its input.

Sequential models. Take MLPs as an example. In this case, each LN is foldable because it directly follows a linear layer, independently of previous layers or input activations. In more complex settings, additional layers may lie between the general linear layer and the target LN. Notably, layer involving only scalar operations (i.e., $\mathbf{x} \mapsto a\mathbf{x}$ for some $a \in \mathbb{R}$) preserve the zero-mean property of the sample. These include scale layers (e.g., dropout layer in inference mode) and constant multiplication layers (e.g., temperature scaling). Therefore, the centering operation in LN can still be folded into the parameters of the preceding linear transformation, even when the scalar operations are interspersed between the general linear layer and the LN.

Parallel Connections. Modern neural networks often contain more complex connections, including parallel branches. Among them, the residual connection sums multiple branches. To eliminate the mean of the output of a residual connection, it is sufficient to eliminate the mean of each branch separately by linearity. Hence, the downstream LN can be folded by applying CBWC to the general linear layers on each branch. In contrast, other parallel connections, such as concatenation, break the required mathematical equivalence and therefore prevent the downstream LN from being foldable. A more detailed proof is provided in Appendix D.1.

To systematically determine whether an LN is foldable in an arbitrary neural network, we next develop a graph-based analysis of how the original parameter space Θ can be effectively folded into a target parameter space Θ^* through CBWC.

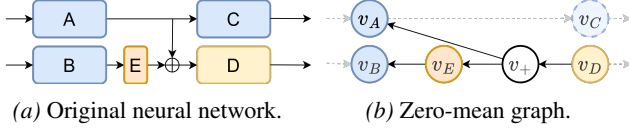


Figure 3. An example network and its associated zero-mean graph. Layer D is an LN, layer E is a scalar operation, and \oplus denotes residual addition. Layer D is foldable if and only if $v_A, v_B \in V_l$.

4.2. Analysis of Neural Networks from a Graph Perspective

We model the network as a directed graph $G = (V, E)$. Each vertex $v \in V$ corresponds to a layer, represented as a function $f : \mathbb{R}^m \rightarrow \mathbb{R}^n$, for some $m, n \in \mathbb{N}_+$. Each directed edge $\langle u, v \rangle \in E \subseteq V \times V$ indicates that the output of layer u is used as an input to layer v .

We denote by $V_l \subseteq V$ the subset of vertices corresponding to general linear layers. We further define $V_s := \{f \mid \forall \mathbf{x} \in \mathbb{R}^m, f(\mathbf{x}) = a \cdot \mathbf{x}, \forall a \in \mathbb{R}\}$ as the set of scalar operations, and $V_r := \{f \mid \forall \mathbf{x}_1, \mathbf{x}_2 \in \mathbb{R}^m, f(\mathbf{x}_1, \mathbf{x}_2) = \mathbf{x}_1 + \mathbf{x}_2, \}$ as the set of residual addition operations. For layers whose outputs are intrinsically zero-mean, we define $V_c := \{f \mid \forall \mathbf{x} \in \mathbb{R}^m, f(\mathbf{x})^\top \mathbf{1}_n = 0\}$. All remaining operations are collected into $V_- := V \setminus (V_l \cup V_s \cup V_r \cup V_c)$. These typically include nonlinear operations such as ReLU or softmax, which in general disrupt the zero-mean property and hence prevent the downstream LN from being foldable.

To determine whether an LN is foldable, we verify whether its input maintains zero mean due to parameter constraints imposed on upstream layers. Starting from the vertex v_{LN} corresponding to the LN, we backtrack along the graph according to the following rules:

- If the predecessor vertex belongs to V_l , zero-mean output can be ensured by applying CBWC.
- If it belongs to V_s , we continue backtracking through its predecessor.
- If it belongs to V_r , we backtrack through all of its input branches.
- If it belongs to V_c , the zero-mean property is already guaranteed.
- If it belongs to V_- , zero mean is not guaranteed, and thus LN folding fails.

Definition 4.2 (Zero-Mean Graph). Given a neural network with computation graph $G = (V, E)$ and a target LN vertex $v_{\text{LN}} \in V$, we recursively construct the corresponding *zero-mean graph* $G_z = (V_z, E_z)$ as follows. Initialize $V_0 = \{u \mid \langle u, v_{\text{LN}} \rangle \in E\}$ and $E_0 = \{\langle v_{\text{LN}}, u \rangle \mid \langle u, v_{\text{LN}} \rangle \in E\}$. For each iteration $k = 0, 1, 2, \dots$:

Algorithm 1 Detect foldable LNs and the corresponding upstream layers requiring CBWC.

```

1: Input: Model  $\mathcal{M}$  with input tensor  $T_0^{\text{in}}$ 
2: Output: Set  $\mathcal{S}$  of foldable LNs and set  $\mathcal{C}$  of corresponding upstream layers requiring CBWC
3:  $T_0^{\text{in}}.\text{centered} \leftarrow \text{False}$  ▷ Initial tensor state.
4:  $\mathcal{S}, \mathcal{C} \leftarrow \emptyset$  ▷ Initialize the output sets.
5: for each step  $t$ , layer  $M_t \in \mathcal{M}$  do ▷ Process the current layer.
6:   if  $T_t^{\text{in}} \leftarrow \sum_{i=1}^n T_i$  then ▷  $T_t^{\text{in}}$  corresponds to a residual connection.
7:      $T_t^{\text{in}}.\text{centered} \leftarrow \bigwedge_{i=1}^n T_i.\text{centered}$ 
8:      $T_t^{\text{in}}.\text{corresponding} \leftarrow \bigcup_{i=1}^n T_i.\text{corresponding}$  ▷ Update the state and corresponding layer set.
9:   end if
10:  if  $M_t = \text{LN}$  and  $T_t^{\text{in}}.\text{centered} = \text{True}$  then
11:     $\mathcal{S} \leftarrow \mathcal{S} \cup \{M_t\}$ 
12:     $\mathcal{C} \leftarrow \mathcal{C} \cup \{T_t^{\text{in}}.\text{corresponding}\}$  ▷ Record the foldable LN and its corresponding layers.
13:  end if
14:   $T_t^{\text{out}} \leftarrow M_t(T_t^{\text{in}})$  ▷ Compute the output tensor.
15:  if  $M_t \in V_s$  then
16:     $T_t^{\text{out}}.\text{centered} \leftarrow T_t^{\text{in}}.\text{centered}$ 
17:     $T_t^{\text{out}}.\text{corresponding} \leftarrow T_t^{\text{in}}.\text{corresponding}$  ▷ Preserve the previous state and set.
18:  else if  $M_t \in V_l \cup V_c$  then
19:     $T_t^{\text{out}}.\text{centered} \leftarrow \text{True}$ 
20:     $T_t^{\text{out}}.\text{corresponding} \leftarrow M_t$  ▷ Update the state and corresponding layer.
21:  else
22:     $T_t^{\text{out}}.\text{centered} \leftarrow \text{False}$ 
23:     $T_t^{\text{out}}.\text{corresponding} \leftarrow \emptyset$  ▷ Reset the state and corresponding layer set.
24:  end if
25: end for
26: Return:  $\mathcal{S}$  and  $\mathcal{C}$ 
    
```

1. Let $A_k = \{v \in V_k \mid v \in (V_r \cup V_s)\}$, i.e., the subset of current leaf vertices that require further backtracking.
2. Define $V_{k+1} = \bigcup_{v \in A_k} \{u \mid \langle u, v \rangle \in E\}$ by backtracking from every vertex in A_k . If $V_{k+1} = \emptyset$, the iteration terminates.
3. Define $E_{k+1} = \bigcup_{v \in A_k} \{\langle v, u \rangle \mid \langle u, v \rangle \in E\}$ by adding the corresponding reversed edges to the graph.

Define $V_z = \bigcup_{k=0}^{\infty} V_k$, $E_z = \bigcup_{k=0}^{\infty} E_k$.

The leaf nodes of a zero-mean graph belong to either V_l , V_c , or V_- . Therefore, the root LN is foldable if all leaf nodes correspond to general linear layers or layers that already guarantee zero-mean output. In that case, the LN

can be replaced with RMSNorm by applying CBWC to the corresponding upstream general linear layers.

For the remaining case in which a leaf node belongs to V_- , zero-mean output can still be enforced by inserting an explicit auxiliary centering operation after that layer, which we discuss as a practical extension. This makes the subsequent LN foldable, provided that the inserted centering does not violate the stricter criterion discussed in Appendix D.2. Although such auxiliary centering introduces extra computational cost, it is still beneficial when the number of resulting foldable LNs exceeds the number of inserted centering operations. Under this practical extension, all LNs in pre-norm and post-norm Transformers (Xiong et al., 2020) can be folded (see Appendix D.3).

4.3. Algorithm for Detecting Foldable LNs

Based on the above analysis, we propose an algorithm for detecting all foldable LNs in arbitrary neural networks and identifying the corresponding upstream layers requiring CBWC. Rather than explicitly backtracking from each LN to form its zero-mean graph, we track the state of each tensor together with its corresponding upstream layers requiring CBWC during a forward traversal. We present Algorithm 1.

Our algorithm automatically detects foldable LNs in arbitrary neural networks and identifies the corresponding upstream general linear layers requiring CBWC to enable mathematically equivalent replacement of LN with RMSNorm. We empirically evaluated Algorithm 1 on mainstream architectures including GPT-2 (Radford et al., 2019), BERT (Devlin et al., 2019), ViT (Dosovitskiy et al., 2021), Phi (Gunasekar et al., 2023), BLOOM (Scao et al., 2022), and OPT (Zhang et al., 2022). Remarkably, all LNs in these models can be folded. We also fold most LNs in VMamba (Liu et al., 2024). Other widely used models such as LLaMA (Touvron et al., 2023) and Mamba2 (Dao & Gu, 2024) employ RMSNorm instead of LN by design. We note that the runtime and memory overhead of the folding procedure is minimal and can be amortized after only a few inference steps. Further details are provided in Appendix E.

5. Experiments

In this section, we empirically evaluate the effectiveness and efficiency of the proposed method. Since our goal is to retain the advantages of LN while reducing its computational cost, we first examine whether the centering operation in LN provides practical benefits over RMSNorm. We then study the performance of CBWC+RMSNorm in training and fine-tuning settings.

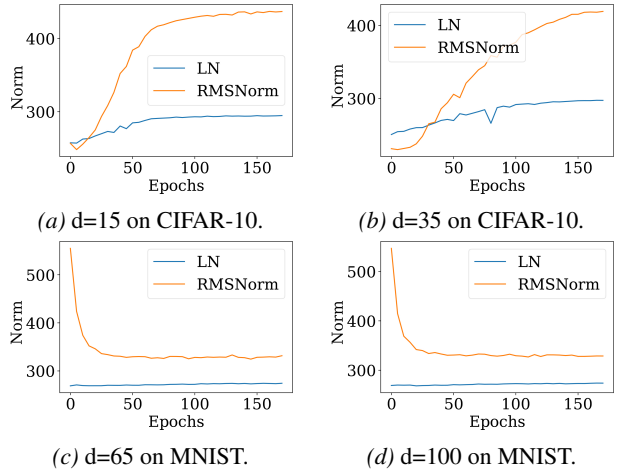


Figure 4. Norm of the input to the final layer for MLPs of different depths (d). LN more effectively controls the sample norm before the final layer throughout training.

5.1. Observation of Centering

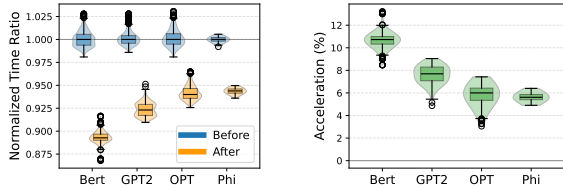
Although the benefits of centering in LN remain debated, we observe that centering helps stabilize the activation range of a network. To examine this effect, we conduct ablation experiments on MLPs of different depths using LN and RMSNorm on the CIFAR-10 (Krizhevsky, 2009) and MNIST (LeCun et al., 1998) classification tasks. We monitor the input statistics of each layer throughout training. Detailed experimental settings and additional results are provided in Appendix F.

As shown in Figure 4, LN keeps the norm of the last layer’s input within a narrower range throughout training. In contrast, without the centering operation, the input mean and norm exhibit substantially larger variations. We also report the variation of input norm across all linear layers in Appendix F, further illustrating the stabilizing role of LN’s centering operation, particularly in the presence of residual connections.

These observations suggest that LN retains practical benefits over RMSNorm that are worth preserving, thereby justifying a structured and theoretically grounded replacement of LN rather than a direct switch to RMSNorm.

5.2. Inference-Time Acceleration

At inference time, CBWC+RMSNorm provides a direct efficiency advantage over standard LN. Notably, CBWC only needs to be applied once to a pre-trained model before deployment, since the weight matrix remains fixed during inference. At the layer level, replacing LN with RMSNorm substantially reduces the cost of normalization, yielding a theoretical latency reduction of roughly 50% to 80% for the normalization step itself. At the whole-model level, this translates into an expected end-to-end runtime reduction of



(a) Normalized time. (b) Acceleration ratio.

Figure 5. Inference latency comparison across four representative models (GPT-2, BERT, OPT, and Phi-3). Both the normalized latency and the acceleration percentage are reported relative to the mean baseline latency of each model.

roughly 4% to 7%, depending on the proportion of LN in the model. More details are provided in Appendix G.1.

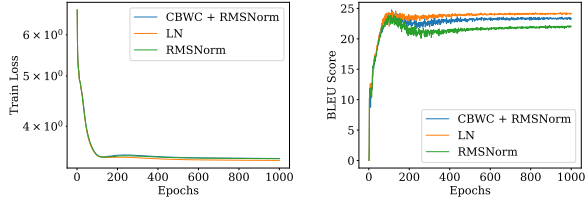
To verify the practical effectiveness of our method, we compare LN with RMSNorm on a single A100-40G GPU. We conduct experiments on GPT-2 (Radford et al., 2019), BERT (Devlin et al., 2019), BLOOM (Scao et al., 2022), OPT (Zhang et al., 2022), and Phi (Gunasekar et al., 2023). Our method reduces end-to-end inference time by approximately 2% to 12% at batch size 2 and sequence length 1024, while preserving identical outputs, as shown in Figure 5.

Although the relative improvement may appear modest, it translates into substantial absolute savings in energy and operational cost when deployed at scale. Additional experiments on both V100 and A100 GPUs show consistent latency reductions of 2.5% to 5.9% together with throughput gains of 1,119 to 3,385 tokens/s across multiple architectures. Moreover, the acceleration becomes more pronounced at longer sequence lengths, with the relative speedup increasing substantially in long-context settings. These results confirm that CBWC+RMSNorm provides a reliable inference-time improvement while preserving equivalence across diverse architectures and deployment scenarios.

5.3. Empirical Study of Training

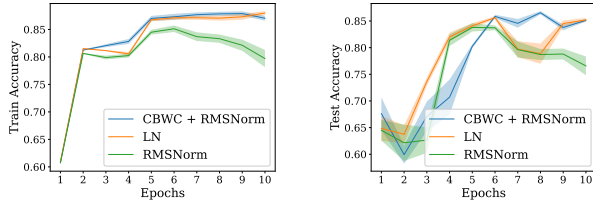
CBWC+RMSNorm can be more efficient than LN during training, especially in long-sequence settings. Let b denote the batch size, s the sequence length, and d the hidden dimension. Let the weight matrix be $W \in \mathbb{R}^{d \times p}$. For one training epoch with B samples, a centering operation incurs a computational cost of approximately $\mathcal{O}(Bsd)$, while CBWC introduces a cost of $\mathcal{O}(Bdp/b)$. Therefore, CBWC is more efficient when $s \times b > p$, which commonly holds in practice, particularly for long-context learning.

Although Prop. 3.2 establishes the theoretical equivalence between a foldable LN and CBWC+RMSNorm during both inference and training, practical Transformer architectures typically include dropout layers (Vaswani et al., 2017) between general linear layers and LN. In training mode, dropout disrupts the zero-mean property of activa-

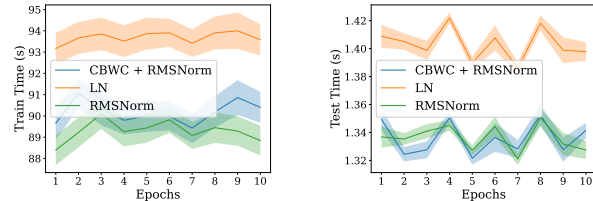


(a) Training loss. (b) Evaluation BLEU.

Figure 6. Training loss curves and validation BLEU scores of Transformer on the Multi30K translation task. Our proposed CBWC+RMSNorm achieves final performance between standard LN and vanilla RMSNorm.



(a) Training accuracy. (b) Test accuracy.



(c) Training time. (d) Test time.

Figure 7. Training and test performance of Transformer-based text classification on the AG News dataset. The results are averaged over 5 random seeds with shaded regions indicating standard deviation. Our CBWC+RMSNorm matches the convergence behavior and final accuracy of standard LN while achieving nearly the same training and inference throughput as vanilla RMSNorm.

tions, thereby breaking exact equivalence. We therefore conduct experiments to empirically evaluate the performance and efficiency of CBWC+RMSNorm on Transformer models. We compare three variants: the baseline with LN, the variant with vanilla RMSNorm, and the variant using our method, CBWC+RMSNorm.

Text Translation. We train the models on the Multi30K (Elliott et al., 2016) dataset following the experimental protocol of Vaswani et al. (2017). We measure training performance using the loss value and evaluate inference performance using BLEU scores (Kishore Papineni & Zhu, 2002). Higher BLEU and lower loss indicate better performance. All models are trained for 1000 epochs. As shown in Figure 6, after the first 100 epochs, vanilla RMSNorm lags behind both the baseline and our method. Although CBWC+RMSNorm is slightly inferior to LN in terms of final training loss and BLEU, it consistently outperforms vanilla RMSNorm.

Table 1. Image classification performance on ImageNet-100 using Swin-Tiny (averaged over 3 random seeds). Our method achieves the best results on both accuracy and loss.

Method	Test Acc (%) \uparrow	Test Loss \downarrow
LN	57.270 \pm 0.060	3.352 \pm 0.015
RMSNorm	57.079 \pm 0.317	3.350 \pm 0.023
CBWC+RMS	57.768 \pm 0.417	3.232 \pm 0.043

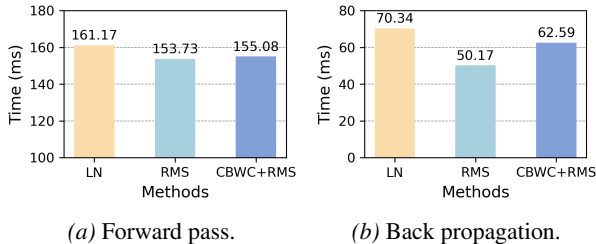


Figure 8. End-to-end latency comparison of Swin-Tiny variants for different processes on ImageNet-100. Our CBWC+RMSNorm delivers markedly lower latency than LN in both forward and backward passes, approaching the efficiency of vanilla RMSNorm.

Text Classification. We train the models on the AG News (Zhang et al., 2015) dataset using the same Transformer setting as in the translation experiment. Each model is trained for 10 epochs with 5 random seeds, and we evaluate both accuracy and time usage. As shown in Figure 7, the baseline and CBWC+RMSNorm both outperform vanilla RMSNorm during training, while RMSNorm exhibits less stable behavior. In terms of efficiency, CBWC+RMSNorm is faster than the LN baseline in both training and evaluation, while remaining close to vanilla RMSNorm.

Image Classification. We conduct image classification experiments on ImageNet-100 (Deng et al., 2009; Chun-Hsiao Yeh, 2022) using Swin-Tiny (Liu et al., 2021). We evaluate both inference performance and runtime efficiency, including forward-pass, backward-pass, and validation time. All models are trained for 100 epochs, and results are averaged over 3 random seeds. Detailed settings are provided in Appendix H.2. As shown in Table 1 and Figure 8, our method achieves the best test performance among the three variants while also improving runtime over the LN baseline. Its latency remains close to that of vanilla RMSNorm in both the forward pass and evaluation.

Summary. When exact folding conditions do not fully hold during training, CBWC+RMSNorm still consistently performs between LN and vanilla RMSNorm, and often remains close to LN in predictive performance while providing noticeable efficiency gains, especially in long-sequence tasks.

Practical Trade-off. The core goal of our method is to reduce the computational cost of LN while preserving its

behavior as much as possible. Therefore, when exact equivalence does not fully hold, whether to apply the method during training or only at inference time becomes a practical design choice. If strict equivalence and no accuracy degradation are required, it is preferable to apply the method only at inference time, for example by converting an LN-trained model after training to accelerate deployment. By contrast, if faster training is preferred and a small performance gap from LN is acceptable, applying the method during training provides a favorable compromise. In practice, this allows one to choose between better fidelity to LN and greater computational efficiency depending on the target use case.

5.4. Discussion on Fine-tuning

In practical applications, models are often fine-tuned from pre-trained checkpoints rather than trained from scratch. Under the conditions of Prop. 3.2, LN and CBWC+RMSNorm follow the same optimization process, and their parameters are mathematically equivalent under the same weight matrix. Therefore, a model pre-trained with LN can in principle be converted and continue training with our method equivalently. We provide a verification experiment for this equivalence in Appendix H.4.1.

We further study the feasibility of applying our method during fine-tuning on Transformer models. In practical settings, however, dropout layers break the exact equivalence between the LN model and the CBWC+RMSNorm model during training. We therefore conduct experiments under three settings: continuing fine-tuning with LN as the baseline, converting the pre-trained model to CBWC+RMSNorm before fine-tuning, and converting the pre-trained model to CBWC while fine-tuning with vanilla RMSNorm. We pre-train GPT-3 Medium (350M) (Brown et al., 2020b) on WikiText-103 (Merity et al., 2016) for 3 epochs and then fine-tune the models on Alpaca (Taori et al., 2023) for 1 epoch. More detailed settings are provided in Appendix H.4.2.

We evaluate the models using loss and perplexity (PPL), where lower values indicate better performance. The results are shown in Table 2. CBWC+RMSNorm achieves the best test loss and perplexity among the compared variants while also benefiting from improved efficiency. These results suggest that applying our method after LN pre-training remains a viable and effective strategy for fine-tuning.

6. Conclusion

We propose a general framework for determining whether an LN in an arbitrary DNN can be replaced with RMSNorm while preserving mathematical equivalence under appropriate structural conditions. We show how the centering operation of LN can be removed through the pro-

Table 2. Fine-tuning performance of GPT-3 Medium (350M) on the Alpaca instruction-following dataset after pre-training on WikiText-103. Our CBWC+RMSNorm achieves the best test loss and perplexity among all variants.

Method	Test Loss ↓	Test PPL ↓
LN	0.2553	1.29
RMSNorm	0.2526	1.29
CBWC+RMS	0.2430	1.28

posed column-centered constraint (CCC) and column-based weight centering (CBWC), and further extend this analysis to arbitrary neural networks through the notions of foldable LN and zero-mean graph. This framework enables exact replacement of foldable LNs during inference with measured end-to-end inference speedups of 2%–12% on representative models and is especially relevant to inference acceleration in LN-based LLMs and VLMs, where exact forward equivalence is particularly desirable. In particular, it provides an effective practical strategy for training and fine-tuning even when the exact folding conditions do not fully hold. More broadly, it offers a principled way to reduce the computational cost of LN while preserving its benefits as much as possible.

Limitations and Future Work. Our analysis and empirical validation, while covering several representative architectures and tasks, do not yet exhaust the full range of modern large-scale models with LN. In future work, it would be valuable to extend the study to a broader set of LLMs and VLMs and to provide more systematic evaluations of the practical gains achieved by the proposed method in different deployment settings. In addition, exact equivalence may fail in architectures containing modules such as dropout, which break the zero-mean property during training. Developing more refined treatments of such modules and extending the framework to a wider class of practical architectures remain important directions for future research.

Acknowledgments

This work was partially supported by Beijing Natural Science Foundation (Grant No. QY24137), National Natural Science Foundation of China (Grant No. 62476016 and 62441617) and the Fundamental Research Funds for the Central Universities.

Impact Statement

This paper presents work whose goal is to advance the field of machine learning. We do not identify any specific negative societal impacts that require particular discussion beyond the general considerations associated with improving the efficiency of deep neural networks.

References

- Abdin, M., Aneja, J., Awadalla, H., Awadallah, A., Awan, A. A., Bach, N., Bahree, A., Bakhtiari, A., Bao, J., Behl, H., et al. Phi-3 technical report: A highly capable language model locally on your phone, 2024. URL <https://arxiv.org/abs/2404.14219>.
- Alayrac, J.-B., Donahue, J., Luc, P., Miech, A., Barr, I., Hasson, Y., Lenc, K., Mensch, A., Millican, K., Reynolds, M., et al. Flamingo: a visual language model for few-shot learning. In *NeurIPS*, 2022.
- Ba, J. L., Kiros, J. R., and Hinton, G. E. Layer normalization, 2016.
- Brown, T., Mann, B., Ryder, N., Subbiah, M., Kaplan, J. D., Dhariwal, P., Neelakantan, A., Shyam, P., Sastry, G., Askell, A., Agarwal, S., et al. Language models are few-shot learners. In *NeurIPS*, 2020a.
- Brown, T. B., Mann, B., Ryder, N., Subbiah, M., Kaplan, J., Dhariwal, P., Neelakantan, A., Shyam, P., Sastry, G., Askell, A., et al. Language models are few-shot learners. *Advances in Neural Information Processing Systems (NeurIPS)*, 33:1877–1901, 2020b.
- Carion, N., Massa, F., Synnaeve, G., Usunier, N., Kirillov, A., and Zagoruyko, S. End-to-end object detection with transformers. In *ECCV*, 2020.
- Cheng, B., Misra, I., Schwing, A. G., Kirillov, A., and Girdhar, R. Masked-attention mask transformer for universal image segmentation. In *CVPR*, 2022.
- Chun-Hsiao Yeh, Y. C. IN100pytorch: Pytorch implementation: Training resnets on imagenet-100. <https://github.com/danielchye/ImageNet-100-Pytorch>, 2022.
- Dai, Z., Yang, Z., Yang, Y., Carbonell, J., Le, Q., and Salakhutdinov, R. Transformer-XL: Attentive language models beyond a fixed-length context. In *ACL*, 2019.
- Dao, T. and Gu, A. Transformers are ssms: Generalized models and efficient algorithms through structured state space duality. *arXiv preprint arXiv:2405.21060*, 2024.
- Deng, J., Socher, R., Fei-Fei, L., Dong, W., Li, K., and Li, L.-J. Imagenet: A large-scale hierarchical image database. In *CVPR*, 2009.
- Devlin, J., Chang, M.-W., Lee, K., and Toutanova, K. BERT: Pre-training of deep bidirectional transformers for language understanding. In *ACL*, 2019.
- Dosovitskiy, A., Beyer, L., Kolesnikov, A., Weissenborn, D., Zhai, X., Unterthiner, T., Dehghani, M., Minderer, M., Heigold, G., Gelly, S., Uszkoreit, J., and Houlsby, N.

- An image is worth 16x16 words: Transformers for image recognition at scale. In *ICLR*, 2021.
- Elliott, D., Frank, S., and Sima'an, K. Multi30k: Multilingual english-german image descriptions. In *ILLC*, 2016.
- Gunasekar, S., Zhang, Y., Aneja, J., Mendes, C. C. T., Giorno, A. D., Gopi, S., Javaheripi, M., Kauffmann, P., de Rosa, G., Saarikivi, O., et al. Textbooks are all you need. *ArXiv*, abs/2306.11644, 2023. URL <https://api.semanticscholar.org/CorpusID:259203998>.
- Huang, L., Liu, X., Liu, Y., Lang, B., and Tao, D. Centered weight normalization in accelerating training of deep neural networks. In *2017 IEEE International Conference on Computer Vision (ICCV)*, pp. 2822–2830, 2017.
- Huang, L., Qin, J., Zhou, Y., Zhu, F., Liu, L., and Shao, L. Normalization techniques in training dnns: Methodology, analysis and application. *IEEE Transactions on Pattern Analysis and Machine Intelligence*, 2023.
- Ioffe, S. and Szegedy, C. Batch normalization: Accelerating deep network training by reducing internal covariate shift. In *ICML*, 2015.
- Jacob, B., Kligys, S., Chen, B., Zhu, M., Tang, M., Howard, A., Adam, H., and Kalenichenko, D. Quantization and training of neural networks for efficient integer-arithmetic-only inference. In *Proceedings of the IEEE Conference on Computer Vision and Pattern Recognition (CVPR)*, June 2018.
- Jiang, Z., Gu, J., Zhu, H., and Pan, D. Pre-rmsnorm and pre-crmsnorm transformers: equivalent and efficient pre-ln transformers. *Advances in Neural Information Processing Systems*, 36:45777–45793, 2023.
- Kirillov, A., Mintun, E., Ravi, N., Mao, H., Rolland, C., Gustafson, L., Xiao, T., Whitehead, S., Berg, A. C., Lo, W.-Y., Dollar, P., and Girshick, R. Segment anything. In *ICCV*, 2023.
- Kishore Papineni, Salim Roukos, T. W. and Zhu, W.-J. Bleu: a method for automatic evaluation of machine translation. In *ACL*, 2002.
- Krizhevsky, A. Learning multiple layers of features from tiny images. 2009.
- LeCun, Y., Kanter, I., and Solla, S. A. Second order properties of error surfaces: Learning time and generalization. In *NeurIPS*, 1990.
- LeCun, Y., Bottou, L., Bengio, Y., and Haffner, P. Gradient-based learning applied to document recognition. *Proceedings of the IEEE*, 86(11):2278–2324, 1998.
- Liu, Y., Tian, Y., Zhao, Y., Yu, H., Xie, L., Wang, Y., Ye, Q., and Liu, Y. Vmamba: Visual state space model. *arXiv preprint arXiv:2401.10166*, 2024.
- Liu, Z., Lin, Y., Cao, Y., Hu, H., Wei, Y., Zhang, Z., Lin, S., and Guo, B. Swin transformer: Hierarchical vision transformer using shifted windows. In *Proceedings of the IEEE/CVF International Conference on Computer Vision (ICCV)*, 2021.
- Mehta, S., Sekhavat, M. H., Cao, Q., Horton, M., Jin, Y., Sun, C., Mirzadeh, I., Najibi, M., Belenko, D., Zatloukal, P., et al. Openelm: An efficient language model family with open-source training and inference framework. *arXiv preprint arXiv:2404.14619*, 2024.
- Merity, S., Xiong, C., Bradbury, J., and Socher, R. Pointer sentinel mixture models, 2016. URL <https://arxiv.org/abs/1609.07843>.
- Montavon, G. and Müller, K.-R. *Deep Boltzmann Machines and the Centering Trick*, volume 7700 of *LNCS*. 2012.
- Nowlan, S., Oja, E., and Amari, S.-I. Natural gradient works efficiently in learning. 1998.
- Radford, A., Narasimhan, K., Salimans, T., Sutskever, I., et al. Improving language understanding by generative pre-training. 2018.
- Radford, A., Wu, J., Child, R., Luan, D., Amodei, D., and Sutskever, I. Language models are unsupervised multitask learners. 2019.
- Raffel, C., Shazeer, N., Roberts, A., Lee, K., Narang, S., Matena, M., Zhou, Y., Li, W., and Liu, P. J. Exploring the limits of transfer learning with a unified text-to-text transformer. *J. Mach. Learn. Res.*, 21(1), jan 2020.
- Raffel, C., Shazeer, N., Roberts, A., Lee, K., Narang, S., Matena, M., Zhou, Y., Li, W., and Liu, P. J. Exploring the limits of transfer learning with a unified text-to-text transformer, 2023. URL <https://arxiv.org/abs/1910.10683>.
- Scao, T. L., Fan, A., Akiki, C., Pavlick, E., and et al, S. I. Bloom: A 176b-parameter open-access multilingual language model. *ArXiv*, abs/2211.05100, 2022. URL <https://api.semanticscholar.org/CorpusID:253420279>.
- Schraudolph, N. N. Accelerated gradient descent by factor-centering decomposition. Technical report, 1998.
- Taori, R., Gulrajani, I., Zhang, T., Dubois, Y., Li, X., Guestrin, C., Liang, P., and Hashimoto, T. B. Stanford alpaca: An instruction-following llama model. https://github.com/tatsu-lab/stanford_alpaca, 2023.

- Team, G., Mesnard, T., Hardin, C., Dadashi, R., Bhupatiraju, S., Pathak, S., Sifre, L., Rivière, M., Kale, M. S., Love, J., et al. Gemma: Open models based on gemini research and technology. *arXiv preprint arXiv:2403.08295*, 2024.
- Tian, Y., Krishnan, D., and Isola, P. Contrastive multiview coding. *arXiv preprint arXiv:1906.05849*, 2019.
- Touvron, H., Lavril, T., Izacard, G., Martinet, X., Lachaux, M.-A., Lacroix, T., Rozière, B., Goyal, N., Hambro, E., Azhar, F., et al. Llama: Open and efficient foundation language models. *arXiv preprint arXiv:2302.13971*, 2023.
- Ulyanov, D., Vedaldi, A., and Lempitsky, V. Instance normalization: The missing ingredient for fast stylization. *arXiv preprint arXiv:1607.08022*, jul 2016. doi: 10.48550/arXiv.1607.08022. URL <https://arxiv.org/abs/1607.08022>.
- Vaswani, A., Shazeer, N., Parmar, N., Uszkoreit, J., Jones, L., Gomez, A. N., Kaiser, L. u., and Polosukhin, I. Attention is all you need. In *NeurIPS*, 2017.
- Wang, B. and Komatsuzaki, A. Gpt-j-6b: A 6 billion parameter autoregressive language model. <https://github.com/kingoflolz/mesh-transformer-jax>, 2021.
- Wu, Y. and He, K. Group normalization. In *Proceedings of the European Conference on Computer Vision (ECCV)*, 2018.
- Xiong, R., Yang, Y., He, D., Zheng, K., Zheng, S., Xing, C., Zhang, H., Lan, Y., Wang, L., and Liu, T.-Y. On layer normalization in the transformer architecture. In *ICML*, 2020.
- Yang, A., Yang, B., Hui, B., Zheng, B., Yu, B., Zhou, C., Li, C., Li, C., Liu, D., Huang, F., et al. Qwen2 technical report, 2024. URL <https://arxiv.org/abs/2407.10671>.
- Zhang, B. and Sennrich, R. Root mean square layer normalization. In *NeurIPS*, 2019.
- Zhang, P., Zeng, G., Wang, T., and Lu, W. Tinyllama: An open-source small language model. *arXiv preprint arXiv:2401.02385*, 2024.
- Zhang, S., Roller, S., Goyal, N., Artetxe, M., Chen, M., Chen, S., Dewan, C., Diab, M., Li, X., Lin, X. V., et al. Opt: Open pre-trained transformer language models. *arXiv preprint arXiv:2205.01068*, 2022.
- Zhang, X., Zhao, J., and LeCun, Y. Character-level convolutional networks for text classification. In *NeurIPS*, 2015.

A. Bias in the Weight Matrix

In the main paper, we omit the bias for simplicity. Here, we provide the methodology for merging the bias into the weight matrix. For a linear layer $\mathbf{h} = \mathbf{W}\mathbf{x} + \mathbf{b}$, we denote the bias $\mathbf{b} = [b_1, b_2, \dots, b_m]^\top \in \mathbb{R}^{m \times 1}$. For simplicity, we append an additional dimension to \mathbf{x} , which turns \mathbf{x} into $\mathbf{x}' = [x_1, x_2, \dots, x_d, 1]^\top \in \mathbb{R}^{(d+1) \times 1}$, and adds an additional column in $\mathbf{W}' \in \mathbb{R}^{m \times (d+1)}$, where:

$$\mathbf{W}' = \begin{bmatrix} w_{1,1} & w_{1,2} & \cdots & w_{1,d} & b_1 \\ w_{2,1} & w_{2,2} & \cdots & w_{2,d} & b_2 \\ \vdots & \vdots & \ddots & \vdots & \vdots \\ w_{n,1} & w_{n,2} & \cdots & w_{n,d} & b_n \end{bmatrix}. \quad (10)$$

Therefore, we have $\mathbf{h} = \mathbf{W}\mathbf{x} + \mathbf{b} = \mathbf{W}'\mathbf{x}'$

In more general cases, for a linear transformation $f(\cdot; \boldsymbol{\theta}) : \mathbb{R}^n \rightarrow \mathbb{R}^m$, we similarly add an additional dimension to $\mathbf{x}' = [x_1, x_2, \dots, x_d, 1]$, and a related weight vector $\mathbf{w}_{d+1} = \mathbf{b} = [b_1, b_2, \dots, b_m]^\top \in \mathbb{R}^m$. Therefore, we have transformed expression:

$$\mathbf{h}(\cdot; \boldsymbol{\theta}) = \sum_{i=1}^d \mathbf{w}_i(\boldsymbol{\theta})x_i + \mathbf{b} = \sum_{i=1}^{d+1} \mathbf{w}_i(\boldsymbol{\theta})x_i, \quad (11)$$

thus incorporating the bias into the weight matrix.

B. Proof of Propositions

B.1. Proof of Prop. 3.1

Proof. For arbitrary input \mathbf{x} , the output is $\mathbf{h} = \sum_{i=1}^n \mathbf{w}_i(\boldsymbol{\theta}_k)x_i$. Taking the mean of \mathbf{h} over the m output neurons,

$$\mu_h = \frac{1}{m} \mathbf{1}_m^\top \mathbf{h} = \frac{1}{m} \sum_{i=1}^n x_i \underbrace{\mathbf{1}_m^\top \mathbf{w}_i(\boldsymbol{\theta}_k)}_{=0} = 0,$$

where the equality follows from CCC equation 6. □

B.2. Proof of Prop. 3.2

Sketch. Let model A have a standard linear layer followed by LN, while model B uses a linear layer with CBWC followed by RMSNorm. In model A , the centered output after LN can be written as $\tilde{\mathbf{h}}_A = \left(\mathbf{I} - \frac{1}{m} \mathbf{1}_m \mathbf{1}_m^\top\right) \mathbf{W}_A \mathbf{x}_A$, where \mathbf{x}_A is the input. In model B , the output is $\tilde{\mathbf{h}}_B = \mathbf{V}_B \mathbf{x}_B = \left(\mathbf{I} - \frac{1}{m} \mathbf{1}_m \mathbf{1}_m^\top\right) \mathbf{W}_B \mathbf{x}_B$. If $\mathbf{x}_A = \mathbf{x}_B$ and $\mathbf{W}_A = \mathbf{W}_B$, then forward outputs are identical.

Since the parameters and outputs coincide, their gradients and losses coincide as well. Therefore, in model A , we have backpropagation process as:

$$\frac{\partial \mathcal{L}}{\partial \mathbf{h}_A} = \left(\mathbf{I} - \frac{1}{m} \mathbf{1}_m \mathbf{1}_m^\top\right)^\top \frac{\partial \mathcal{L}}{\partial \tilde{\mathbf{h}}_A}, \quad \frac{\partial \mathcal{L}}{\partial \mathbf{x}_A} = \mathbf{W}_A^\top \frac{\partial \mathcal{L}}{\partial \mathbf{h}_A}, \quad \frac{\partial \mathcal{L}}{\partial \mathbf{W}_A} = \frac{\partial \mathcal{L}}{\partial \mathbf{h}_A} \mathbf{x}_A^\top. \quad (12)$$

When in model B , according to the definition of backward transformation ψ in CBWC, similarly we have:

$$\frac{\partial \mathcal{L}}{\partial \mathbf{x}_B} = \mathbf{V}_B \frac{\partial \mathcal{L}}{\partial \tilde{\mathbf{h}}_B}, \quad \frac{\partial \mathcal{L}}{\partial \mathbf{V}_B} = \frac{\partial \mathcal{L}}{\partial \tilde{\mathbf{h}}_B} \mathbf{x}_B^\top, \quad \frac{\partial \mathcal{L}}{\partial \mathbf{W}_B} = \left(\mathbf{I} - \frac{1}{m} \mathbf{1}_m \mathbf{1}_m^\top\right)^\top \frac{\partial \mathcal{L}}{\partial \mathbf{V}_B}. \quad (13)$$

It is straightforward to verify that the two backpropagation processes are identical:

$$\frac{\partial \mathcal{L}}{\partial \mathbf{x}} = \left(\mathbf{I} - \frac{1}{m} \mathbf{1}_m \mathbf{1}_m^\top\right)^\top \mathbf{W}^\top \frac{\partial \mathcal{L}}{\partial \tilde{\mathbf{h}}}, \quad \frac{\partial \mathcal{L}}{\partial \mathbf{W}} = \left(\mathbf{I} - \frac{1}{m} \mathbf{1}_m \mathbf{1}_m^\top\right)^\top \frac{\partial \mathcal{L}}{\partial \tilde{\mathbf{h}}} \mathbf{x}^\top. \quad (14)$$

Therefore, CBWC+RMSNorm yields an identical optimization process. □

C. Column-Based Weight Centering of General Linear Layers

In this section, we introduce the column-based weight transformation (CCWT) and give the explicit definition of general linear layers. We provide how typical general linear layers can be converted into a linear transformation, including recurrent layers and convolution layers, and derive their corresponding CCC and CBWC. We further provide the grouped-CCC and grouped CBWC for group normalization.

C.1. Column-Centered Weight Transformation

To achieve the CCC of a general linear layer in inference and ensure a subsequent LN foldable, we propose *column-centered weight transformation*. The aim of CCC is to fold centering operation (in Eqn.4) into linear layer. Notice that given a layer input vector $\mathbf{x} = [x_1, x_2, \dots, x_n]^\top \in \mathbb{R}^n$, the centering operation can be written into the form of $\tilde{\mathbf{x}} = \left(\mathbf{I} - \frac{1}{m} \mathbf{1}_m^\top \mathbf{1}_m\right) \mathbf{x}$, where the matrix $\left(\mathbf{I} - \frac{1}{m} \mathbf{1}_m^\top \mathbf{1}_m\right)$ can be moved into the linear layer.

We have the definition below.

Definition C.1 (Column-Centered Weight Transformation (CCWT)). *Column-centered weight transformation* aims to apply transformation on the weight matrix to ensure column-centered constraint. We construct a specific transformation φ , changes \mathbf{W} into \mathbf{W}' , as:

$$\mathbf{W}' = \varphi(\mathbf{W}) = \left(\mathbf{I} - \frac{1}{m} \mathbf{1}_m^\top \mathbf{1}_m\right) \mathbf{W}, \quad (15)$$

where m is the output neuron number.

Apparently, CCWT ensures that the weight for each input in the transformed matrix \mathbf{W}' has zero mean, thus guarantees CCC and ensures a zero-mean output of the layer. For different general linear layers, the transformation Ψ takes different forms, but the essence of its construction based on column-centered constraint will not change.

CBWC is a special transformation on the parameter, folding the parameter space onto that of CCC while maintaining mathematical equivalence of the original model. With the construct of CCWT, it becomes easier to get the form of CBWC. For a given CCWT, we transfer it to CBWC by using a proxy weight in the place of \mathbf{W}' . Instead of directly replacing the computational weight \mathbf{V} , we ensure \mathbf{V} is under column-centered constraint while \mathbf{W} is calculated from \mathbf{V} by CCWT.

C.2. General Linear Layer

In the main paper, we introduce the concept of general linear layer, which apply linear transformations to their inputs. Recurrent layers with shared weights in RNNs and convolution layers in CNNs are all general linear layers as they satisfy additivity and homogeneity. We formalize the definition of general linear layer as follows.

Definition C.2 (General Linear Layers). A layer parameterized by θ with transformation $\mathbf{h}(\mathbf{x}; \theta)$, where $\mathbf{x} \in \mathbb{R}^n$, is a *general linear layer* if the mapping $\mathbf{h}(\cdot; \theta)$ satisfies additivity and homogeneity:

- $\mathbf{h}(\mathbf{x}_1 + \mathbf{x}_2; \theta) = \mathbf{h}(\mathbf{x}_1; \theta) + \mathbf{h}(\mathbf{x}_2; \theta), \forall \mathbf{x}_1, \mathbf{x}_2 \in \mathbb{R}^n$.
- $\mathbf{h}(c\mathbf{x}; \theta) = c \mathbf{h}(\mathbf{x}; \theta), \forall \mathbf{x} \in \mathbb{R}^n, c \in \mathbb{R}$.

Namely, the transformation $\mathbf{h}(\mathbf{x}; \theta)$ satisfies linearity, and is a linear transformation of \mathbf{x} .

Such layers can be explicitly expressed as the form of $\mathbf{h}(\mathbf{x}; \theta) = \mathbf{W}(\theta)\mathbf{x}$, allowing for direct application of CCC and CBWC.

C.2.1. RECURRENT LAYER

Despite linearity, the recurrent neural network is different from the original linear layer with its recurrent connection and shared weight matrix. Due to the fact that our constraints are independent of input and output, the parameter sharing is excluded from our consideration. As for the recurrent connection, the weights for ordinary input and recurrent input can be seen as two linear layers.

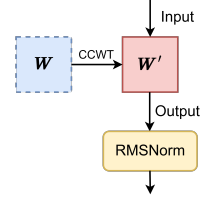


Figure 9. Sketch map of CCWT.

For the l -th layer and t -th time step of a recurrent neural network, we define the input as $\mathbf{x}_t^{l-1} \in \mathbb{R}^{d_{l-1}}$, the recurrent input as $\mathbf{h}_{t-1}^l \in \mathbb{R}^{d_l}$ and the output of the hidden layer as \mathbf{c}_t^l . We have the weight matrix $\mathbf{W}_v = [\mathbf{w}_1^v, \dots, \mathbf{w}_{d_{l-1}}^v] \in \mathbb{R}^{d_l \times d_{l-1}}$ and $\mathbf{W}_h = [\mathbf{w}_1^h, \dots, \mathbf{w}_{d_l}^h] \in \mathbb{R}^{d_l \times d_l}$, where $\mathbf{w}_i^v, \mathbf{w}_i^h \in \mathbb{R}^{d_{l-1}}$ and which is shared between all time steps. We define $\mathbf{W} = [\mathbf{W}_v, \mathbf{W}_h]$ and input $\mathbf{x} = [(\mathbf{x}_t^{l-1})^\top, (\mathbf{h}_{t-1}^l)^\top]^\top$. We have recurrent layer in form of a linear transformation as follows:

$$\mathbf{c}_t = \mathbf{h}_{\text{rnn}}(\mathbf{x}; \mathbf{W}) = \mathbf{W}_v \mathbf{x}_t^{l-1} + \mathbf{W}_h \mathbf{h}_{t-1}^l, \quad (16)$$

where we have $\mathbf{w}_i(\mathbf{W}) = \mathbf{w}_i^v$ when $i = 1, \dots, d_{l-1}$ and $\mathbf{w}_i(\mathbf{W}) = \mathbf{w}_{i-d_{l-1}}^h$ when $i = (d_{l-1} + 1), \dots, (d_{l-1} + d_l)$. Therefore, we have the constraint:

$$\mathbf{W}_0 \in \Theta_{\text{rnn}} = \left\{ \mathbf{W} : (\mathbf{w}_j^v)^\top \cdot \mathbf{1}_{d_l} = \sum_{i=1}^{d_l} w_{i,j}^v = 0, (\mathbf{w}_j^h)^\top \cdot \mathbf{1}_{d_l} = \sum_{i=1}^{d_l} w_{i,k}^h = 0, \right. \\ \left. j = 1, 2, \dots, d_{l-1}, k = 1, 2, \dots, d_l \right\}. \quad (17)$$

Under the constraint of Eqn. 17, we have the mean of output with:

$$\begin{aligned} \mu_t^c &= \frac{1}{d_l} \sum_{i=1}^{d_l} \left(\sum_{j=1}^{d_{l-1}} w_{i,j}^v x_j + \sum_{k=1}^{d_l} w_{i,k}^h h_k \right) \\ &= \frac{1}{d_l} \left(\sum_{j=1}^{d_{l-1}} \left(\sum_{i=1}^{d_l} w_{i,j}^v \right) x_j + \sum_{k=1}^{d_l} \left(\sum_{i=1}^{d_l} w_{i,k}^h \right) h_k \right) \\ &= \frac{1}{d_l} \left(\sum_{j=1}^{d_{l-1}} 0 \cdot x_j + \sum_{k=1}^{d_l} 0 \cdot h_k \right) = 0. \end{aligned} \quad (18)$$

Thus, for the shared weight matrix for both input from the last layer and from the last time step, applying constraints on them centralizes the output of the hidden layer. We have the transformation $\varphi_{\text{rnn},v}, \varphi_{\text{rnn},h}$ of the CCWT on the recurrent neural network, as follows:

$$\begin{aligned} \mathbf{W}^{lv} &= \varphi_{\text{rnn},v}(\mathbf{W}^v) = \left(I - \frac{1}{m_v} \mathbf{1}_{m_v} \mathbf{1}_{m_v}^\top \right) \mathbf{W}^v \\ \mathbf{W}^{lh} &= \varphi_{\text{rnn},h}(\mathbf{W}^h) = \left(I - \frac{1}{m_h} \mathbf{1}_{m_h} \mathbf{1}_{m_h}^\top \right) \mathbf{W}^h. \end{aligned} \quad (19)$$

We have the corresponding CBWC for the recurrent layer as below:

$$\begin{aligned} \mathbf{V}^v &= \varphi_{\text{rnn},v}(\mathbf{W}^v) = \left(I - \frac{1}{m_v} \mathbf{1}_{m_v} \mathbf{1}_{m_v}^\top \right) \mathbf{W}^v, \\ \mathbf{V}^h &= \varphi_{\text{rnn},h}(\mathbf{W}^h) = \left(I - \frac{1}{m_h} \mathbf{1}_{m_h} \mathbf{1}_{m_h}^\top \right) \mathbf{W}^h, \\ \frac{\partial \mathcal{L}}{\partial \mathbf{W}^v} &= \phi_{\text{rnn},v} \left(\frac{\partial \mathcal{L}}{\partial \mathbf{V}} \right) = \left(I - \frac{1}{m_v} \mathbf{1}_{m_v} \mathbf{1}_{m_v}^\top \right)^\top \frac{\partial \mathcal{L}}{\partial \mathbf{V}}, \\ \frac{\partial \mathcal{L}}{\partial \mathbf{W}^h} &= \phi_{\text{rnn},h} \left(\frac{\partial \mathcal{L}}{\partial \mathbf{V}} \right) = \left(I - \frac{1}{m_h} \mathbf{1}_{m_h} \mathbf{1}_{m_h}^\top \right)^\top \frac{\partial \mathcal{L}}{\partial \mathbf{V}}. \end{aligned} \quad (20)$$

C.2.2. CONVOLUTION LAYER

Under the circumstances of the convolution layer, the convolution kernel can be regarded as a combination of a set of shared weights. All of them should fulfill the constraint of the linear layer. We hence use a vector to denote the elements among different channels among the kernel.

We denote the input tensor $\mathbf{x} \in \mathbb{R}^{d_{l-1} \times h \times w}$ and the output tensor $\mathbf{H} \in \mathbb{R}^{d_l \times h' \times w'}$. We have convolution kernels $\mathbf{W} \in \mathbb{R}^{d_l \times d_{l-1} \times F_h \times F_w}$.

For every channel of output tensor $\mathbf{H}_i \in \mathbb{R}^{h' \times w'}$ ($i = 1, \dots, d_l$), every channel of input tensor $\mathbf{x}_j \in \mathbb{R}^{h \times w}$ ($j = 1, \dots, d_{l-1}$) and corresponding convolution kernel $\mathbf{w}_{i,j} \in \mathbb{R}^{F_h \times F_w}$ ($i = 1, \dots, d_l$, $j = 1, \dots, d_{l-1}$), we have:

$$\mathbf{H}_k = \sum_{t=1}^{d_{l-1}} \mathbf{x}_t * \mathbf{w}_{k,t}. \quad (21)$$

For more specifics, we have:

$$h_{k,i,j} = \sum_{t=1}^{d_{l-1}} \sum_{a=1}^{F_h} \sum_{b=1}^{F_w} x_{t,(is-s-p+a-1),(js-s-p+b-1)} \cdot w_{k,t,a,b}, \quad (22)$$

where the subscript sequence refers to the order number of the element in each dimension. Obviously, this equation can be written into the form of a linear transformation:

$$\mathbf{H} = \mathbf{h}_{\text{cnn}}(\mathbf{x}; \mathbf{W}) = \sum_{t=1}^{d_{l-1}} \sum_{a=1}^h \sum_{b=1}^w \mathbf{w}_{t,a,b}(\mathbf{W}) \cdot x_{t,a,b}. \quad (23)$$

Therefore, we have the constraint:

$$\mathbf{W}_0 \in \Theta_{\text{cnn}} = \left\{ \mathbf{W} : \sum_{i=1}^{d_l} \mathbf{w}_{i,j} = \mathbf{0}, j = 1, 2, \dots, d_{l-1} \right\}. \quad (24)$$

Due to the convolution operation, we have $a * (b + c) = a * b + a * c$. Thus, under the constraint of Eqn.24, we have:

$$\begin{aligned} \mu_h &= \frac{1}{d_l} \sum_{i=1}^{d_l} \mathbf{H}_i = \frac{1}{d_l} \sum_{i=1}^{d_l} \sum_{j=1}^{d_{l-1}} \mathbf{x}_j * \mathbf{w}_{i,j} = \frac{1}{d_l} \sum_{j=1}^{d_{l-1}} \mathbf{x}_j * \left(\sum_{i=1}^{d_l} \mathbf{w}_{i,j} \right) \\ &= \frac{1}{d_l} \sum_{j=1}^{d_{l-1}} \mathbf{x}_j * \mathbf{0} = 0. \end{aligned} \quad (25)$$

It thus can be seen that the column-centered constraint on the convolution kernels achieves the effect of the centering of the LN. We have the transformation φ_{cnn} of the CCWT on convolution layers, as follows:

$$\mathbf{W} = \varphi_{\text{cnn}}(\mathbf{W}) = \left(\mathbf{I} - \frac{1}{h \times w} \mathbf{1}_{h \times w}^\top \mathbf{1}_{h \times w} \right) \mathbf{W}. \quad (26)$$

To be noted, the tensor \mathbf{W} here is a four-dimension tensor. The transformation here is to do centering on its second dimension.

We have a corresponding CBWC for the convolution layer as below:

$$\begin{aligned} \mathbf{V} &= \varphi_{\text{cnn}}(\mathbf{W}) = \left(\mathbf{I} - \frac{1}{h \times w} \mathbf{1}_{h \times w}^\top \mathbf{1}_{h \times w} \right) \mathbf{W}. \\ \frac{\partial \mathcal{L}}{\partial \mathbf{W}} &= \varphi_{\text{cnn}} \left(\frac{\partial \mathcal{L}}{\partial \mathbf{V}} \right) = \left(\mathbf{I} - \frac{1}{h \times w} \mathbf{1}_{h \times w} \mathbf{1}_{h \times w}^\top \right)^\top \frac{\partial \mathcal{L}}{\partial \mathbf{V}}. \end{aligned} \quad (27)$$

C.3. Grouped Column-Centered Constraint For GN

We extend the conclusion to Group Normalization (GN) (Wu & He, 2018). Group normalization is first defined on the channel dimension for convolution input $\mathbf{X} \in \mathbb{R}^{d \times h \times w}$. So the Group Normalization here is more similar to grouped Layer Normalization, with the definition below:

Definition C.3 (Group Normalization (GN)). Suppose the number of groups is g , and $d = g \times c$. Let $\mathbf{x} = [z_1^\top, \dots, z_g^\top]^\top$, where $z_i = [z_{i1}, \dots, z_{ic}]^\top$, ($i = 1, \dots, g$). Assuming $\mathbf{x} = [x_1, \dots, x_d]^\top$, we denote $z_{ij} = x_{(i-1) \times c + j}$. Let $\hat{\mathbf{x}} = GN(\mathbf{x})$, where $GN(\cdot)$ denotes the *group normalization*. GN can be calculated by $\mu_i = (z_{i1} + \dots + z_{ic})/c$, $\sigma_i^2 = [(z_{i1} - \mu_i)^2 + \dots + (z_{ic} - \mu_i)^2]/c$, and then $\hat{z}_{ij} = (z_{ij} - \mu_i)/\sigma_i$. Thus, we have $\hat{\mathbf{x}} = [\hat{z}_1^\top, \dots, \hat{z}_g^\top]^\top$, where $\hat{z}_i = LN(z_i)$, ($i = 1, \dots, g$).

For every input, we divide the neurons into groups and apply normalization in every group. Thus the centering step in this normalization is to ensure the output sum of all neurons in each group is zero. For a sampled input $\mathbf{h} = [h_1, h_2, \dots, h_m]^\top$, for g groups and c channels in every group ($g \times c = m$), we have:

$$\mu_{hj} = \frac{1}{c} \sum_{i=1}^c h_{ji} = 0 \quad (j = 1, \dots, g). \quad (28)$$

For a given general linear layer The parameter θ_0 is under column-centered constraint of GN if θ_0 satisfies:

$$\theta_0 \in \Sigma = \{ \theta : \mathbf{w}_i^\top(\theta) \cdot \mathbf{1}_{(c, k \times c)} = 0, k = 1, 2, \dots, n \}. \quad (29)$$

Take the linear layer $\mathbf{h} = \mathbf{W}\mathbf{x}$ as an example, we have the weight matrix $\mathbf{W} = [\mathbf{w}_1, \mathbf{w}_2, \dots, \mathbf{w}_{d_{l-1}}] \in \mathbb{R}^{d_l \times d_{l-1}}$, where $\mathbf{w}_i \in \mathbb{R}^{d_l}$, $i = 1, \dots, d_{l-1}$. Similarly, we have $\mathbf{w}_i(\mathbf{W}) = \mathbf{w}_i$. Therefore, the column-centered constraint for GN can be expressed as:

$$\mathbf{W}_0 \in \Sigma_{GN} = \left\{ \mathbf{W} : \sum_{k=1}^c w_{j, (k+c \times i)} = 0, i = 1, 2, \dots, g, j = 1, 2, \dots, d \right\}. \quad (30)$$

Given $\mathbf{h} = \mathbf{W}\mathbf{x}$, for the i -th neuron output h_i in the j -th group of \mathbf{h} , we have:

$$h_i = \sum_{k=1}^d w_{i,j} \cdot x_j. \quad (31)$$

Under the constraint of Eqn. 30, we have:

$$\mu_{hj} = \frac{1}{c} \sum_{i=1}^c h_{ji} = \frac{1}{c} \sum_{i=1}^c \sum_{j=1}^d w_{i,j} \cdot x_j = \frac{1}{c} \sum_{j=1}^d \left(\sum_{i=1}^c w_{i,j} \right) x_j = \frac{1}{c} \sum_{j=1}^d 0 \cdot x_j = 0. \quad (32)$$

Thus, we replace the centering step of GN with a grouped column-centered constraint. To be mentioned, the core idea of designing a constraint is to ensure every group of input weight has zero mean.

For the transformation φ_{GN} of the CCWT on a normal linear layer under GroupNorm, we have:

$$\mathbf{W} = \varphi_{GN}(\mathbf{W}) = (\mathbf{I} - \mathbf{A})\mathbf{W}. \quad (33)$$

\mathbf{A} is a matrix that we construct with the equation below:

$$\mathbf{A} = \mathbf{I} - \frac{1}{c} \sum_{k=0}^{d-1} \mathbf{1}_{(c, k \times c)}^\top \mathbf{1}_{(c, k \times c)}, \quad (34)$$

where $\mathbf{1}_{(c, k \times c)}$ refers to a vector whose elements are all zero except that the $(k \times c)$ -th element to $(k \times c + c)$ -th element are ones. Specifically, \mathbf{A} is a matrix with its diagonal arrayed with $c \times c$ matrices of ones.

We have a corresponding grouped CBWC for the linear layer as below:

$$\begin{aligned} \mathbf{V} &= \varphi_{GN}(\mathbf{W}) = (\mathbf{I} - \mathbf{A})\mathbf{W} \\ \frac{\partial \mathcal{L}}{\partial \mathbf{W}} &= \phi_{GN} \left(\frac{\partial \mathcal{L}}{\partial \mathbf{V}} \right) = (\mathbf{I} - \mathbf{A})^\top \frac{\partial \mathcal{L}}{\partial \mathbf{V}}. \end{aligned} \quad (35)$$

It is worth mentioning that InstanceNorm (Ulyanov et al., 2016) is simply the special case where the number of groups g equals the number of channels.

In addition, folding fails when the number of parameters influencing a single output element is smaller than the group size g (which can occur in certain shallow or highly grouped settings). In such cases, the grouped column-centered constraint becomes over-constrained and cannot be satisfied.

Beyond GroupNorm, any normalization (or post-processing) that consists solely of additive (among elements of the sample) and scalar multiplication operations applied per sample can be folded into the preceding general linear layer using the same principle.

C.4. Discussion of Column-Based Weight Centering and Weight Decay Technology

According to the definition of weight decay, this technology involves adding a penalty term based on the L2 norm of the model weights to the original loss function, thereby encouraging the optimizer to favor smaller weight values and improving the model’s generalization performance.

In our method, the model contains two weight matrices. This is because CBWC is implemented by re parameterization: the matrix (\mathbf{V}) used for forward/backward calculation is different from the updated parameter matrix (\mathbf{W}), but the two matrices are connected by deterministic and differentiable transformations (as described in Definition 3.2). The L2 norm of the calculation matrix \mathbf{V} and the storage parameter matrix \mathbf{W} are slightly different. Therefore, two implementation methods of weight decay are derived from this transformation.

Standard implementations (including PyTorch) apply weight decay to the trainable parameters (\mathbf{W} in our case). However, whether weight decay should technically be applied to \mathbf{V} or \mathbf{W} is an interesting and subtle question. Applying it to \mathbf{W} preserves the classic regularization interpretation (penalizing the magnitude of stored parameters), while applying it to \mathbf{V} would more directly penalize the magnitude of the pre-activation weights.

Both choices are defensible, and the community has not reached a consensus of a better choice, which is also orthogonal to the core contribution of our paper. Our discussed implementation (decay on \mathbf{W}) follows PyTorch’s default behavior and does not alter the intended regularization effect in practice.

D. Algorithm for Detecting Foldable LN

D.1. Parallel Connection

In this section, we prove how to fold an LN while the sample meets residual structure during backtracking and provide the reason why other parallel connection fails to fold a downstream LN.

D.1.1. RESIDUAL STRUCTURE

Here we consider a two branch residual structure as an example. The conclusion remains unchanged when the number of branches increases. For a residual structure, we define the input $\mathbf{x} \in \mathbb{R}^n$ and the output $\mathbf{y} \in \mathbb{R}^m$, as shown below:

$$\mathbf{y} = \mathcal{F}(\mathbf{x}; \boldsymbol{\theta}_F) + \mathcal{G}(\mathbf{x}; \boldsymbol{\theta}_G), \tag{36}$$

where both $\mathcal{F}(\cdot; \boldsymbol{\theta}_F)$ and $\mathcal{G}(\cdot; \boldsymbol{\theta}_G)$ are subnetworks, and $\boldsymbol{\theta}_F$ and $\boldsymbol{\theta}_G$ are learnable parameters. Due to the complexity of $\mathcal{F}(\cdot)$, it is intuitively difficult to construct a constraint on this function to eliminate the mean of $\mathcal{G}(\mathbf{x})$. Therefore, we treat the two terms separately and apply constraint based on their content each.

To eliminate the mean of \mathbf{y} , we have $\mathbf{y}' = (I - \frac{1}{m} \mathbf{1}_m \mathbf{1}_m^\top) \mathbf{y}$. According to the distributive law of multiplication, we have:

$$\mathbf{y}' = (I - \frac{1}{m} \mathbf{1}_m \mathbf{1}_m^\top) \mathbf{y} = (I - \frac{1}{m} \mathbf{1}_m \mathbf{1}_m^\top) \mathcal{F}(\mathbf{x}; \boldsymbol{\theta}_F) + (I - \frac{1}{m} \mathbf{1}_m \mathbf{1}_m^\top) \mathcal{G}(\mathbf{x}; \boldsymbol{\theta}_G), \tag{37}$$

Such that, the residual structure has zero-mean output if the output of each branch has zero mean.

D.1.2. OTHER PARALLEL CONNECTION

Other parallel connections do not satisfy linearity, such that we cannot transfer the zero-mean property to each branch.

Take concatenation as an example. When all composite vectors for concatenation have zero mean, stacking vectors along the axis produces a zero-mean tensor. But this zero-mean property of composite vectors and output vectors are not mathematically equivalent in back propagation, thus preventing the downstream LN from folding.

To put this another way, for a concatenation operation, we define the input $\mathbf{x}_i \in \mathbb{R}^{n_i}, i = 1, \dots, n$ and the output $\mathbf{y} \in \mathbb{R}^m$, where $m = \sum_{i=1}^n n_i$, as shown below:

$$\mathbf{y} = f(\mathbf{x}_1, \dots, \mathbf{x}_n) = [\mathbf{x}_1, \dots, \mathbf{x}_n]. \quad (38)$$

To eliminate the mean of \mathbf{y} , we have $\mathbf{y}' = (I - \frac{1}{m} \mathbf{1}_m \mathbf{1}_m^\top) \mathbf{y}$. It is obvious that:

$$\mathbf{y}' = (I - \frac{1}{m} \mathbf{1}_m \mathbf{1}_m^\top) \mathbf{y} \neq [(I - \frac{1}{m} \mathbf{1}_m \mathbf{1}_m^\top) \mathbf{x}_1, \dots, (I - \frac{1}{m} \mathbf{1}_m \mathbf{1}_m^\top) \mathbf{x}_n]. \quad (39)$$

Such that zero mean of each composite vector does not equal to the zero mean of the output vector. Therefore, we cannot fold the downstream LN into the concatenation.

D.2. A Stricter Criteria of Foldable LN

As proposed in the previous section, we can replace the LN with RMSNorm if layers corresponding to the upstream vertices in zero-mean graph are all general linear layers. However, the zero-mean output will be propagated indiscriminately to all connected layers of the upstream layers, which may lead to nonequivalent output and unexpected results.

To ensure mathematical equivalence, we expect all the layers requiring CBWC to affect only LNs. Here we define the *affected layer*.

Definition D.1 (Affected layer). Given a neural network $G = (V, E)$ and the zero-mean graph $G_z = (V_z, E_z)$ for v_{LN} . We initialize $V_0 = \{u \notin V_z \mid \forall v \in (V_z \setminus V_{LN}), \langle v, u \rangle \in E\}$ and $A_0 = \emptyset$. For each iteration $k = 0, 1, 2, \dots$:

1. Let $A_{k+1} = (V_k \cap (V_c \cup V_l \cup V_-))$, update affected layers.
2. Let $V_{k+1} = \{u \mid v \in (V_k \setminus (V_c \cup V_l \cup V_-)), \langle u, v \rangle \in E\}$, trace the next layer through forward pass.

We define $A = \bigcup_{k=0}^{\infty} A_k$ as affected layer.

If the affected layers only include LN, then the zero-mean activation in the zero-mean graph safely ensures a foldable LN. We note that the commonly used models nowadays, such as transformers, all meet this requirement.

D.3. Self-Attention Module and Transformer Structure

D.3.1. SELF-ATTENTION MODULE

To be mentioned, self-attention module can be seen as a pile of layers. We make use of its posterior linear component and thus construct the constraint on it.

For a sampled input $\mathbf{x} \in \mathbb{R}^{n \times d}$, we apply three different learnable weight matrices $\mathbf{Q}, \mathbf{K} \in \mathbb{R}^{d \times d_k}, \mathbf{V} \in \mathbb{R}^{d \times d_v}$ and have three input matrices $\mathbf{H}_Q, \mathbf{H}_K \in \mathbb{R}^{n \times d_k}, \mathbf{H}_V \in \mathbb{R}^{n \times d_v}$ with:

$$\mathbf{H}_Q = \mathbf{x} \cdot \mathbf{Q}, \quad \mathbf{H}_K = \mathbf{x} \cdot \mathbf{K}, \quad \mathbf{H}_V = \mathbf{x} \cdot \mathbf{V}. \quad (40)$$

According to the definition of scaled dot-product attention, we have:

$$\text{Attention}(\mathbf{H}_Q, \mathbf{H}_K, \mathbf{H}_V) = \text{softmax} \left(\frac{\mathbf{H}_Q \mathbf{H}_K^\top}{\sqrt{d_k}} \right) \mathbf{H}_V. \quad (41)$$

When this expression is expanded, it is written as:

$$\text{Attention}(\mathbf{x}; \mathbf{Q}, \mathbf{K}, \mathbf{V}) = \text{softmax} \left(\frac{\mathbf{x} \cdot \mathbf{Q} \cdot \mathbf{K}^\top \cdot \mathbf{x}^\top}{\sqrt{d_k}} \right) \mathbf{x} \cdot \mathbf{V}. \quad (42)$$

To simplify, we denote:

$$\mathbf{B} = \text{softmax} \left(\frac{\mathbf{x} \cdot \mathbf{Q} \cdot \mathbf{K}^\top \cdot \mathbf{x}^\top}{\sqrt{d_k}} \right) \mathbf{x} \in \mathbb{R}^{n \times d}. \quad (43)$$

We can see this module as a linear transformation $\mathbf{h} = \mathbf{h}_{\text{trans}}(\mathbf{B}, \mathbf{V}) = \mathbf{B}\mathbf{V}$, where \mathbf{B} is the input. We denote $\mathbf{B} = [\mathbf{b}_1^\top, \dots, \mathbf{b}_d^\top]^\top$, where $\mathbf{b}_i^\top \in \mathbb{R}^n, i = 1, \dots, d$ and $\mathbf{V} = [\mathbf{v}_1, \dots, \mathbf{v}_d]^\top \in \mathbb{R}^{d \times d_v}$, where $\mathbf{v}_i \in \mathbb{R}^{d_v}, i = 1, \dots, d$.

We have $\mathbf{h} = \mathbf{h}_{\text{trans}}(\mathbf{B}, \mathbf{V}) = \sum_{i=1}^d \mathbf{v}_i \cdot \mathbf{b}_i$ and $\mathbf{w}_i(\mathbf{V}) = \mathbf{v}_i$. Therefore, we have the constraint:

$$\mathbf{W}_0 \in \Gamma_{\text{trans}} = \left\{ \mathbf{W} : \mathbf{v}_i^\top \cdot \mathbf{1}_{d_v} = \sum_{k=1}^{d_v} v_{j,k} = 0, i = 1, 2, \dots, d_{l-1} \right\}. \quad (44)$$

By Eqn. 44, we have

$$\begin{aligned} \mu_a &= \sum_{b=1}^{d_v} (\mathbf{B}\mathbf{H}\mathbf{V})_{(a,b)} = \sum_{b=1}^{d_v} \sum_{j=1}^n b_{a,j} \cdot \mathbf{H}_{V(j,b)} = \sum_{b=1}^{d_v} \sum_{j=1}^n b_{a,j} \left(\sum_{k=1}^d x_{j,k} \cdot v_{k,b} \right) \\ &= \sum_{b=1}^{d_v} \sum_{j=1}^n \sum_{k=1}^d b_{a,j} \cdot x_{j,k} \cdot v_{k,b} = \sum_{j=1}^n \sum_{k=1}^d b_{a,j} \cdot x_{j,k} \left(\sum_{b=1}^{d_v} v_{k,b} \right) \\ &= \sum_{j=1}^n \sum_{k=1}^d b_{a,j} \cdot x_{j,k} \cdot 0 = 0. \end{aligned} \quad (45)$$

Accordingly, we have the transformation φ_{trans} of the CCWT on self-attention modules, as follows:

$$\mathbf{W}^v = \varphi_{\text{trans}}(\mathbf{W}^v) = \left(\mathbf{I} - \frac{1}{m_v} \mathbf{1}_{m_v}^\top \mathbf{1}_{m_v} \right) \mathbf{W}^v. \quad (46)$$

We have a corresponding CBWC for the attention module as below:

$$\begin{aligned} \mathbf{W}^v &= \varphi_{\text{trans}}(\mathbf{W}^v) = \left(\mathbf{I} - \frac{1}{m_v} \mathbf{1}_{m_v}^\top \mathbf{1}_{m_v} \right) \mathbf{W}^v. \\ \frac{\partial \mathcal{L}}{\partial \mathbf{W}} &= \phi_{\text{trans}} \left(\frac{\partial \mathcal{L}}{\partial \mathbf{V}} \right) = \left(\mathbf{I} - \frac{1}{m_v} \mathbf{1}_{m_v} \mathbf{1}_{m_v}^\top \right)^\top \frac{\partial \mathcal{L}}{\partial \mathbf{V}}. \end{aligned} \quad (47)$$

Moreover, multi-head attention modules contain an extra linear layer at the last. Simply applying CCC and CBWC of the linear layer onto it ensures zero-mean output.

D.3.2. POST-LN TRANSFORMER

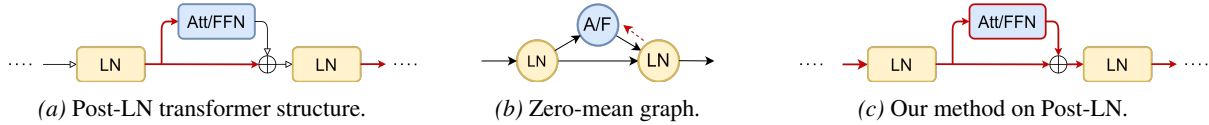


Figure 10. The proof and application of our method on Post-LN. ‘Att’ and ‘FFN’ refer to the Attention layer and the Feed-Forward Network, which are both general linear layers.

For the post-LN transformer, the residual structure connects an LN and a self-attention module or a feed-forward network layer. Obviously, all the LNs are foldable.

D.3.3. PRE-LN TRANSFORMER

Although the embedding block does not provide zero-mean output, an auxiliary centering operation can be inserted after it. For most models like GPT2, there is an LN after the last transformer block. In this case, all downstream LNs can be folded by applying CBWC to the attention and feed-forward layers. Therefore, all LNs in the pre-LN Transformer can be folded under the practical extension. This is also the main idea of the previous paper (Jiang et al., 2023).

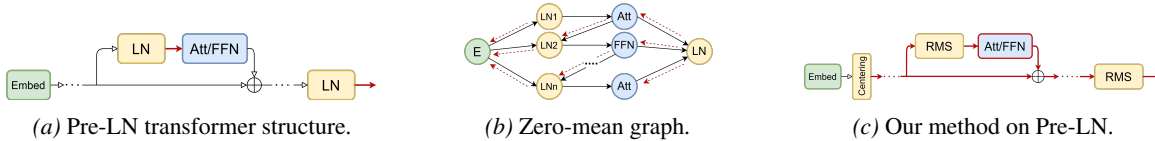


Figure 11. The proof and application of our method on Pre-LN. ‘Att’ and ‘FFN’ refers to the Attention layer and Feed-Forward Network, which are both general linear layers. ‘Embed’ refers to the Embedding layer, which it is not.

E. Implementation Details of Algorithm 1

E.1. Foldable LN in Common Models

Here, we list 11 common models and the number of LN and foldable LN in Table 3. Notice that some models follow the pre-norm Transformer architecture and some LNs can be folded under the practical extension. The models we mentioned here are GPT-2 (Radford et al., 2019), BERT (Devlin et al., 2019), ViT (Dosovitskiy et al., 2021), Phi (Gunasekar et al., 2023), OPT (Zhang et al., 2022), BLOOM (Scao et al., 2022) and VMamba (Liu et al., 2024).

Table 3. Number of LN and foldable LN in 11 common models.

Model	Total	Foldable	Percentage	Foldable (Practical)	Percentage
GPT-2	25	0	0	25	100.00%
BERT	25	24	96.00%	25	100.00%
ViT	25	0	0	25	100.00%
Phi	25	0	0	25	100.00%
OPT	25	0	0	25	100.00%
BLOOM	6	5	83.33%	6	100.00%
VMamba	51	0	0	36	70.59%

To be mentioned, Phi3 (Abdin et al., 2024), Qwen2 (Yang et al., 2024), T5 (Raffel et al., 2023), Mamba2 (Dao & Gu, 2024) and LLaMA (Touvron et al., 2023) originally use RMSNorm, instead of LN.

E.2. Runtime and Memory Overhead

The runtime and memory overhead of our automatic folding algorithm is minimal. The detection phase requires only one forward pass to determine which LN layers are foldable, after which we store a small list mapping foldable layers to their corresponding modules.

Here, we conduct extensive experiments on different models, hardware, batch size and sequence lengths. All inference comparisons use PyTorch’s official fused CUDA LayerNorm as the baseline, and our optimized CUDA RMSNorm kernel derived from it, which we have open-sourced.

We first conduct a confirmatory experiment on GPT-2 using a single RTX 3050 Laptop GPU. The folding algorithm takes 0.0347 seconds. For inference with batch size 32 and sequence length 512, the inference time is reduced from 0.2189 s to 0.2023 s (averaged over 100 runs), yielding a 7.6% speedup. Notably, the memory overhead introduced by the folding algorithm itself is only 19.00 MB (which is released after folding), and the total tensor memory of the model remains unchanged (486.70 MB both before and after folding). These results demonstrate that our method achieves meaningful inference acceleration without any increase in model memory footprint.

To provide a broader empirical picture, we conduct additional experiments. We record time usage and memory usage for Bert, GPT2, OPT and Phi, on A100-40GB and V100-32GB. The batch size and sequence length for inference are 1 and 256 respectively. Memory footprint remains identical before and after folding. We list the results in the tables below:

(a) Fold = Folding time. (b) Init = Model initialize time. (c) Ratio = Fold / (Fold + Init) × 100%. (d) Before = Inference latency without folding. (e) After = Inference latency with algorithm applied. (f) Speedup = (Before - After) / Before × 100%. (g) Break-even = Fold / (Before - After).

The one-time folding algorithm (~60–100 ms on A100, ~100-200 ms on V100) is fully amortized after only a few inference steps in any real deployment. Importantly, larger batch sizes and longer sequences achieve greater acceleration with our

Table 4. Overhead and inference time benefits of folding algorithm on A100-32G GPU.

Model	Fold (s)	Init (s)	Ratio (%)	Before (s)	After (s)	Speedup (%)	Break-even
Bert	0.0452	2.4056	1.84	0.0077	0.0073	5.19	112.9
GPT2	0.0651	3.0651	2.08	0.0119	0.0113	5.22	105.0
OPT	0.0484	2.6283	1.81	0.0092	0.0078	14.60	36.1
Phi	0.0928	22.2692	0.42	0.0531	0.0507	4.52	38.7

Table 5. Overhead and benefits of folding algorithm on V100-32G GPU.

Model	Fold (s)	Init (s)	Ratio (%)	Before (s)	After (s)	Speedup (%)	Break-even
Bert	0.1263	2.0772	5.73	0.0095	0.0086	9.47	140.4
GPT2	0.1639	2.6343	5.86	0.0115	0.0110	4.34	327.8
OPT	0.1183	2.2988	4.90	0.0106	0.0091	14.73	75.6
Phi	0.1779	21.8865	0.81	0.0693	0.0668	3.54	72.6

algorithm in inference, thus requiring fewer runs to break even on the algorithm cost.

Moreover, time usage of folding algorithm is theoretically independent of batch size and sequence length. We conduct experiments on Bert on V100, evaluated the algorithm time usage across six batch sizes (4 to 128) and four sequence lengths (64 to 4096). The result is listed below.

Table 6. Folding algorithm time usage (ms) across different batch sizes (BS) and sequence lengths (SL).

BS\SL	64	256	1024	4096	Average	Std	CV (%)
4	132.3	132.8	133.7	138.4	134.3	2.77	2.06
8	137.1	132.9	133.9	136.9	135.2	2.11	1.56
16	139.3	134.8	134.9	136.0	136.3	2.11	1.55
32	134.6	135.5	136.1	137.6	135.9	1.26	0.92
64	142.7	136.7	138.3	142.0	139.9	2.86	2.04
128	135.9	132.1	136.0	145.1	137.3	5.51	4.01
Average	137.0	134.2	135.5	139.3	136.5	\	\
Std	3.65	1.80	1.73	3.50	\	3.28	\
CV (%)	2.66	1.34	1.28	2.51	\	\	2.40

As shown in Table 6, despite a 2048-fold increase in the total number of processed tokens, the standard deviation of algorithm time usage across all 24 configurations is only 3.3 ms, with a coefficient of variation of merely 2.40%. Both marginal averages (per row and per column) and their corresponding CV values remain below 4%, confirming that algorithm time usage is essentially independent of both batch size and sequence length in practical deployment scenarios.

F. Ablation Experiment of Centering Operation

For the ablation experiments on the centering operation in LN in Section 5.1, we build up simple MLPs by stacking linear layers, LNs and ReLUs. The depth of MLP (i.e., the number of linear layers) varies among 6, 15, and 35 on CIFAR-10 (Krizhevsky, 2009), with a width of 256 and 512. We introduce the residual structure to help converge for deeper MLP with a depth of 65 and 100 on MNIST (LeCun et al., 1998), with a width of 512. We train the model with a learning rate of 0.01 and a batch size of 256. We train all the models for 175 epochs. The training accuracy of all the models in this experiment is 100%.

We show the plot of the input norm of last layer during the training process in Figure 4. Here, we also provide the input mean value of the last layer in Figure 12. Since it is quite close to the change of the input norm, we will not go into detail.

Additionally, we recorded the input norms of every linear layer across all layers for the four models in the final training epoch in Figure 13. The results are summarized as follows:

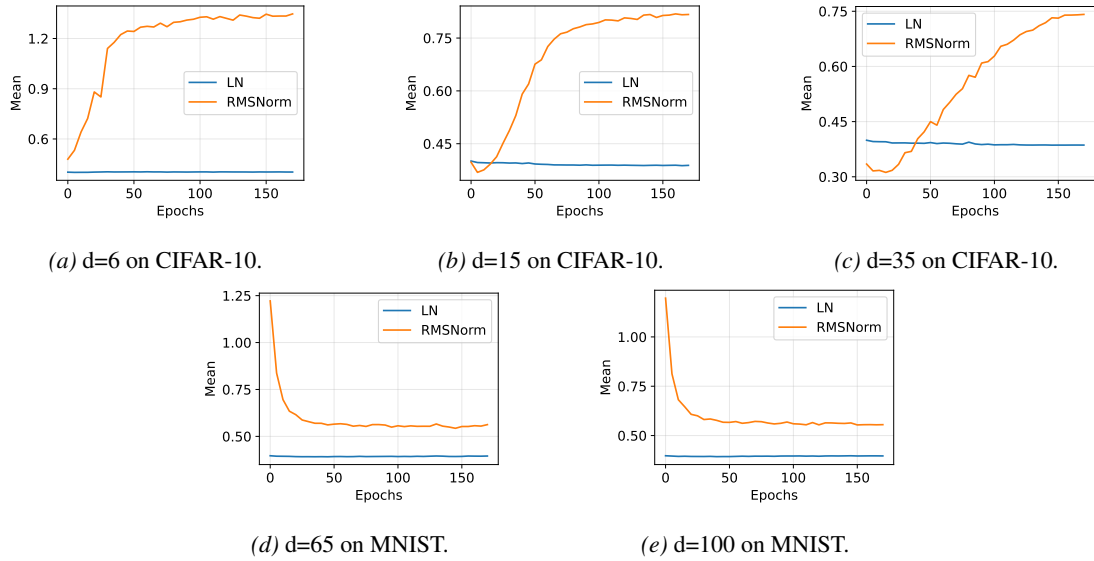


Figure 12. Mean of the final layer's input for MLPs of different depth (d). The change is similar to the change of norm.

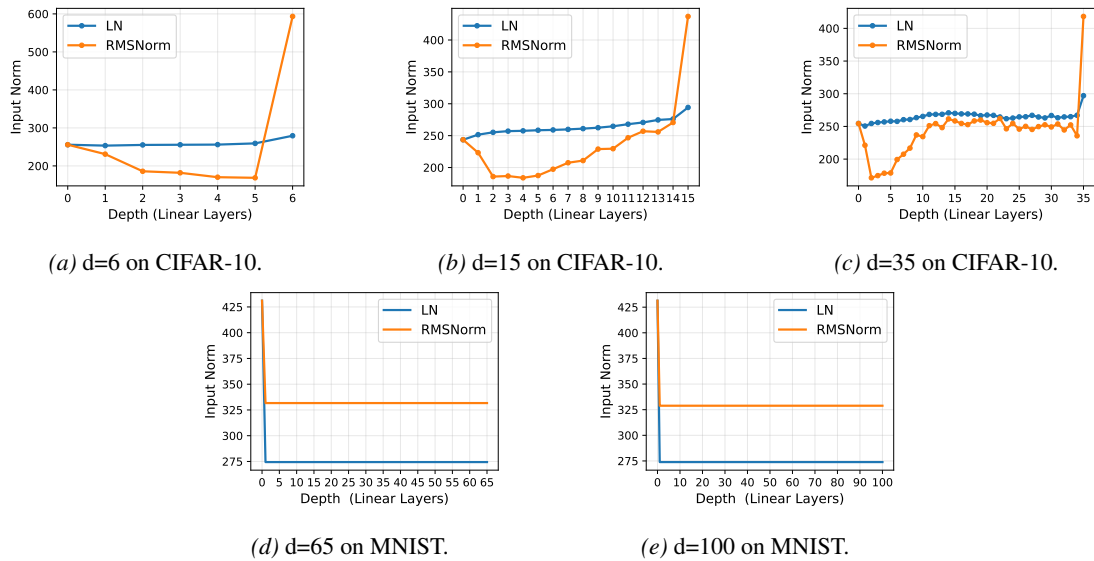


Figure 13. Norm of the input across linear layers for MLPs of different depth (d). LN better controls the norm of samples throughout the model.

- In plain MLP networks (without residual connections), the input norms of the LN model are not strictly smaller than those of RMSNorm at every layer. However, the RMSNorm-based models exhibit a sharp spike in input norm at the final layer, accompanied by clear oscillations in input norms between layers.
- In residual-connected MLP networks, the LN model consistently shows significantly smaller input norms than RMSNorm at every single layer. Moreover, these input norms remain remarkably stable and nearly constant across layers—an effect directly induced by the residual connections.

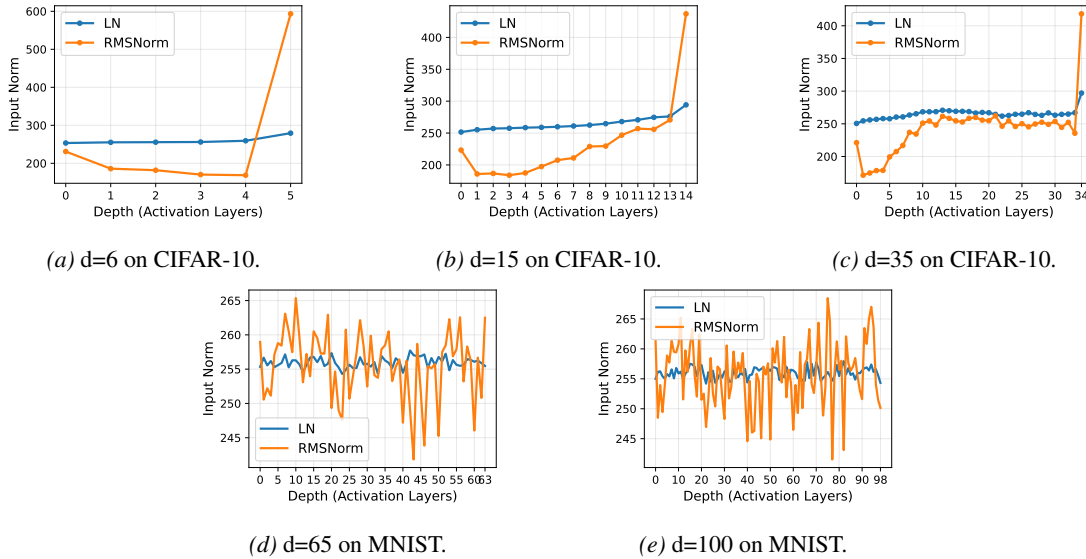


Figure 14. Norm of the input across activation layers for MLPs of different depth d . The change is similar to the change of norm.

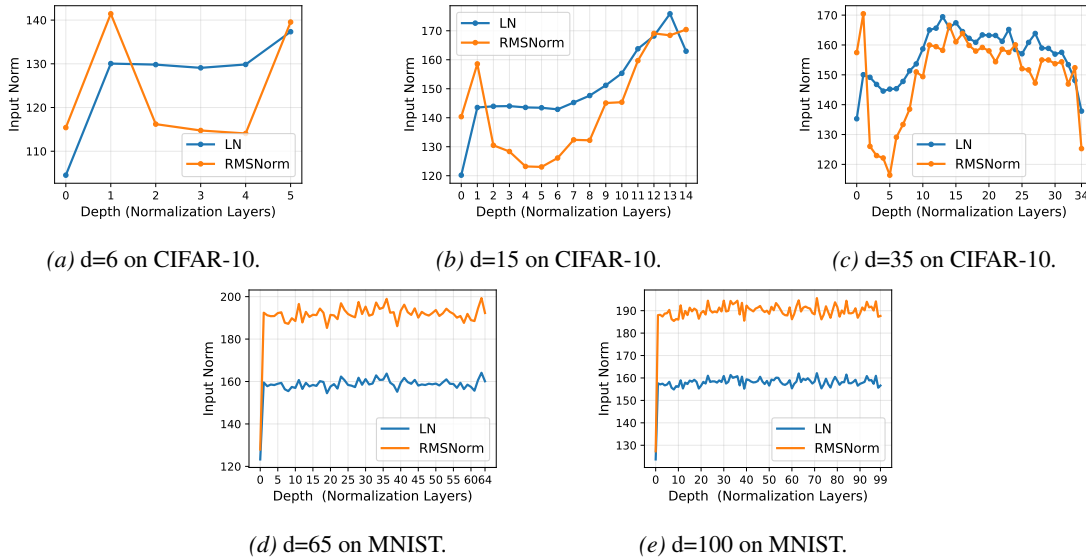


Figure 15. Norm of the input across normalization layers for MLPs of different depth d .

We also observed the variations in input norms across other layers. As depicted in Figure 14, the trend observed in activation function layers is similar to that in linear layers, which we will not elaborate on further. To be noted, the range of input norm with residual connection is actually relatively small, between 240 and 270. As for the normalization layers shown in Figure 15, without residual connections, the range of input norms under RMSNorm exhibits more significant fluctuations, and the inter layer oscillations are greater; in the presence of residual connections, the input norms are effectively constrained by LN.

Therefore, we believe that the centering operation of LN controls the range of activations both across layers and throughout the training process.

G. Inference Acceleration

In this section, we analyze the inference-time acceleration brought by CBWC+RMSNorm, both theoretically and empirically. Since CBWC is applied only once before deployment and the weight matrix remains fixed during inference, the runtime gain mainly comes from replacing LN with RMSNorm.

G.1. Theoretical Analysis

Theoretically, since calculating RMSNorm has fewer computational steps compared to LN, replacing LN with RMSNorm has acceleration in FLOPs, thus reflecting on throughput.

G.1.1. LAYER-LEVEL FLOPS ANALYSIS

FLOPs (Floating-Point Operations) measure the total number of floating-point operations required for one forward pass and are a standard metric for evaluating the computational cost of a model. Although FLOPs are decoupled from the number of parameters, they directly affect inference latency and energy consumption, and are therefore widely used in efficiency-oriented research.

We assume that addition, subtraction, and multiplication each cost one clock tick, while division costs three clock ticks.

Consider a sample \mathbf{x} of dimension d . LN and RMSNorm are defined as follows:

$$\text{LN}(\mathbf{x}) = \frac{\mathbf{x} - \mu}{\sqrt{\sigma^2 + \epsilon}}, \quad \text{where} \quad \mu = \frac{1}{d} \sum_{i=1}^d x_i, \quad \sigma^2 = \frac{1}{d} \sum_{i=1}^d (x_i - \mu)^2. \quad (48)$$

$$\text{RMS}(\mathbf{x}) = \frac{\mathbf{x}}{\sqrt{\sigma_{rms}^2 + \epsilon}}, \quad \text{where} \quad \sigma_{rms}^2 = \frac{1}{d} \sum_{i=1}^d x_i^2. \quad (49)$$

According to the formulas above, we compute the operation counts in Table 7. For a d -dimensional sample, LN requires $5d$ additions, $2d$ multiplications, and d divisions, whereas RMSNorm requires only d additions, $2d$ multiplications, and d divisions. This indicates a clear layer-level computational advantage for RMSNorm.

Table 7. FLOPs calculation for LN and RMSNorm.

Steps	LN			RMS		
	+/-	×	÷	+/-	×	÷
Calculating average (μ)	$d - 1$	0	1	—	—	—
Calculating variance (σ^2)	$2d - 1$	d	1	$d - 1$	d	1
Inverse square root for variance	One <code>rsqrt</code> , ignored					
Centering & scaling for each dimension	d	0	d	0	0	d
Affine	d	d	0	0	d	0
Total	$5d$	$2d$	d	d	$2d$	d

G.1.2. WELFORD-BASED FLOPS ANALYSIS

In practice, PyTorch implements fused LN using the Welford algorithm, whose operation count differs from the naive formulation. We therefore also compare LN and RMSNorm under a Welford-style implementation, which better reflects practical GPU execution.

Instead of traversing the data twice, this method requires only one traversal, with the following updates:

$$\begin{aligned} \bar{x}_{n+1} &= \bar{x}_n + \frac{x_{n+1} - \bar{x}_n}{n + 1}, \\ \widetilde{\sigma}_{n+1}^2 &= \widetilde{\sigma}_n^2 + (x_{n+1} - \bar{x}_n)(x_{n+1} - \bar{x}_{n+1}), \end{aligned} \quad (50)$$

where \bar{x}_n and $\widetilde{\sigma}_n^2 = n\sigma_n^2$ denote the mean and the scaled variance of the first n elements.

For parallel computation, we combine two groups M and N with m and n elements through

$$\begin{aligned}\bar{x}^{(M\cup N)} &= \frac{m}{m+n}\bar{x}^{(M)} + \frac{n}{m+n}\bar{x}^{(N)}, \\ \widetilde{\sigma}^{(M\cup N)} &= \widetilde{\sigma}^{(M)} + \widetilde{\sigma}^{(N)} + \frac{mn}{m+n}\left(\bar{x}^{(M)} - \bar{x}^{(N)}\right)^2.\end{aligned}\tag{51}$$

Similarly, RMSNorm under the same computation pattern can be written as

$$\widetilde{\sigma}_{n+1}^2 = \widetilde{\sigma}_n^2 + x_{n+1}^2,\tag{52}$$

and

$$\widetilde{\sigma}^{(M\cup N)} = \widetilde{\sigma}^{(M)} + \widetilde{\sigma}^{(N)},\tag{53}$$

which are substantially simpler than the corresponding updates for LN.

According to the formulas above, we compute the operation counts in Table 8. For a d -dimensional sample divided into g groups for parallel computation, LN requires $7d$ additions, $3d + 7g$ multiplications, and d divisions, whereas RMSNorm requires only d additions and $3d$ multiplications.

Table 8. FLOPs calculation for LN and RMSNorm under the Welford algorithm.

Steps	Times	LN			RMS		
		+/-	\times	\div	+/-	\times	\div
Group initialization (x_1^2)	g	0	1	0	0	1	0
Summing within groups	$d - g$	5	1	1	1	1	0
Combining groups	$g - 1$	5	7	1	1	0	0
Inverse square root for variance	1	One <code>rsqrt</code> , ignored					
Centering & scaling for each dimension	d	1	1	0	0	1	0
Affine	d	1	1	0	0	1	0
Total	—	$7d$	$3d + 7g$	d	d	$3d$	0

Although the Welford algorithm increases the theoretical FLOPs compared with the naive formulation, it reduces traversal overhead and enables efficient fused GPU execution in practice. Under this implementation, the estimated normalization-layer latency is reduced from approximately $13d + 7g$ clock ticks for LN to $4d$ for RMSNorm, corresponding to a theoretical reduction of roughly 60% to 80% for the normalization step itself.

A similar improvement is expected for throughput. Since our method mainly removes the centering operation and does not significantly change model size or memory footprint, the throughput gain is primarily determined by the reduction in computational latency. Therefore, the throughput trend is expected to be consistent with the latency analysis above.

G.1.3. FROM LAYER-LEVEL SAVINGS TO MODEL-LEVEL SPEEDUP

Although the normalization layer itself can be substantially accelerated, the end-to-end model speedup depends on the fraction of inference time originally spent in LN. We therefore estimate the average proportion of LN latency in several representative models and combine it with the layer-level savings above to obtain an expected whole-model speedup.

We estimate the average inference-time proportion of LN by running each model 1000 times on a single RTX 3090 GPU. Based on the Welford-style analysis above, we expect RMSNorm to provide a 50% to 80% reduction for the normalization layer itself. The resulting estimated end-to-end speedups are shown in Table 9.

G.2. Reference Experiment with Custom LN and RMSNorm

Previous work (Jiang et al., 2023) compared custom implementations of LN and RMSNorm that directly follow Eqns. 48 and 49. Such comparisons are useful as a reference, but they do not reflect real deployment settings, because PyTorch

Table 9. Estimated end-to-end inference speedup from LN time proportion in representative models.

Model	Total Time Usage	LN Time Usage	Proportion	Expected Acceleration
GPT-2	7.125218	0.763676	10.72%	~ 6.5%
BERT	7.462299	0.713215	9.56%	~ 6%
BLOOM	2.321148	0.191480	8.25%	~ 5%
OPT	10.14867	0.743909	7.33%	~ 4.5%
ViT	6.552383	0.766613	11.70%	~ 7%

already provides a highly optimized fused LN kernel, whereas RMSNorm requires a dedicated optimized implementation to be competitive.

In this reference experiment, both LN and RMSNorm are implemented by our team without vendor-level acceleration. As a result, neither implementation reflects the optimized inference kernels used in practice. In particular, a custom LN implementation is substantially slower than PyTorch’s fused LN, which causes LN to occupy an unrealistically large proportion of total model runtime. Moreover, the gap between LN and RMSNorm under this setting differs from the Welford-based comparison in Table 8. We therefore report this experiment only as a reference point, including both runtime and CUDA memory statistics.

Table 10. Average total and CUDA runtime (ms) and acceleration percentage for 16 runs across 6 models using custom LN and custom RMSNorm implementations.

Model	Total Runtime			CUDA Runtime		
	Folded	Original	Acceleration	Folded	Original	Acceleration
GPT-2	10.929	11.923	8.34%	2.784	2.933	5.07%
BERT	11.949	12.916	7.49%	2.904	3.146	7.70%
BLOOM	3.322	3.548	6.38%	0.246	0.285	13.59%
OPT	12.363	12.692	2.59%	2.932	2.994	2.08%
Phi	32.005	32.556	1.69%	26.290	26.691	1.50%
ViT	10.709	11.683	8.34%	4.457	4.723	5.64%

Table 10 shows speedups ranging from roughly 2% to 12%, depending on the LN proportion and model structure. We also report CUDA memory usage in Table 11, where the measured memory reduction ranges from roughly 0.5% to 8.5%.

Table 11. Average CUDA memory usage (Bytes) and reduction percentage for 16 runs across 6 models using custom LN and custom RMSNorm implementations.

Model	Folded	Original	Reduction
GPT-2	303602176	313445376	3.140%
BERT	119192576	129035776	7.628%
BLOOM	7358976	7558656	2.642%
OPT	161150976	161939968	0.487%
Phi	1350695936	1376923136	1.905%
ViT	163479552	178634752	8.484%

G.3. Main CUDA Verification Experiments

G.3.1. MAIN SETTING AND PRIMARY RESULTS

We compare our custom CUDA-accelerated RMSNorm kernel against PyTorch’s official fused LN implementation, which serves as the strongest practical baseline. PyTorch’s LN already incorporates a highly optimized fused implementation, whereas its RMSNorm support is not a comparably strong baseline for this purpose. Therefore, we implement our own CUDA RMSNorm kernel using the same Welford algorithm as fused LN, yielding a comparison that is much closer to the

practical upper bound of achievable inference speedup.

We use `torch.profiler` to trace both total runtime and CUDA runtime. For each model, we conduct 16 runs, each averaged over 100 independent inference passes. The measured runtime of each run is normalized by the mean baseline runtime of the corresponding model. Due to limited hardware resources, the start times of different comparison groups are not perfectly aligned, which introduces some variability in measured runtime.



Figure 16. Inference latency comparison across six representative models (GPT-2, BERT, BLOOM, OPT, Phi-3, and ViT). Our CBWC+RMSNorm achieves a consistent end-to-end runtime reduction of 2%–12% with no accuracy degradation.

We also measure the proportion of inference runtime originally spent in LN for these models, as reported in Table 12.

Table 12. Average inference runtime (ms) and LN proportion in representative models.

Model	Total Time Usage	LN Time Usage	Proportion
BERT	7.462299	0.713215	9.56%
BLOOM	2.321148	0.191480	8.25%
GPT-2	7.125218	0.763676	10.72%
OPT	10.14867	0.743909	7.33%
ViT	6.552383	0.766613	11.70%

The inference performance of BERT, GPT-2, Phi, and OPT in Section 5.2 was evaluated on a single NVIDIA A100-40GB GPU. We first performed 50 warm-up inferences, followed by 15 runs of 50 measured inferences each. All measurements used a fixed batch size of 2 and an input/output sequence length of 1024 tokens.

For analysis, we first computed the mean baseline runtime for each run, and then normalized all measurements within that run against this baseline. The reported acceleration percentages were computed accordingly.

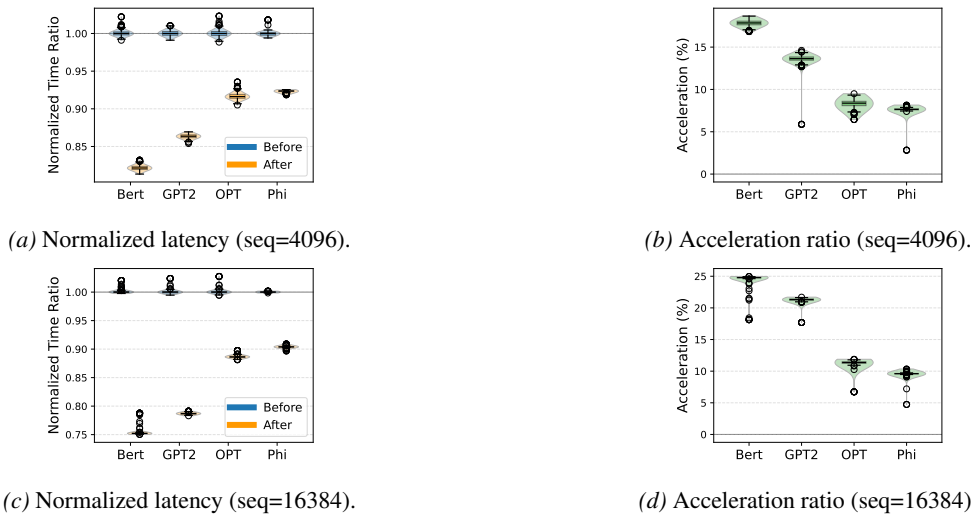


Figure 17. Inference latency comparison under longer sequence lengths. Our CBWC+RMSNorm achieves larger end-to-end speedups as sequence length increases.

We further investigate performance at longer sequence lengths of 4096 and 16384 tokens with a fixed batch size of 2. As shown in Figure 17, the acceleration becomes more pronounced under these conditions, which is consistent with the theoretical analysis.

G.3.2. LATENCY AND THROUGHPUT ON A100 AND V100

We evaluate the inference latency and throughput of BERT, GPT-2, and OPT on single NVIDIA V100-32GB and A100-40GB GPUs.

Table 13. Average inference latency (seconds) on a single GPU with batch size 2 and sequence length 256. Results are averaged over 5 runs, each with 50 measured inferences after 50 warm-up steps.

Model	Hardware	Original Inference Time (s)	New Inference Time (s)	Acceleration (%)
BERT	V100	0.0116	0.0111	3.90
GPT-2	V100	0.0121	0.0117	3.57
OPT	V100	0.0119	0.0116	2.53
BERT	A100	0.0090	0.0087	2.79
GPT-2	A100	0.0093	0.0089	4.22
OPT	A100	0.0094	0.0089	5.85

Table 14. Average inference throughput (tokens/second) on a single GPU with batch size 2 and sequence length 256. Results are averaged over 5 runs, each with 50 measured inferences after 50 warm-up steps.

Model	Hardware	Original Throughput (tokens/s)	New Throughput (tokens/s)	Δ (tokens/s)
BERT	V100	44329.0	46126.1	+1797.1
GPT-2	V100	42199.0	43760.7	+1561.7
OPT	V100	43144.9	44263.9	+1119.0
BERT	A100	57117.4	58756.0	+1638.7
GPT-2	A100	55351.4	57787.8	+2436.5
OPT	A100	54468.1	57853.1	+3385.0

All measurements were performed with a fixed batch size of 2 and input/output sequence length of 256 tokens. To ensure stable timing, we first performed 50 warm-up inferences, followed by 50 measured inferences, and repeated the full process 5 times for each configuration. Total inference time was measured using Python’s `time.time()`.

As shown in Table 13 and Table 14, the proposed method consistently reduces inference latency by 2.5%–5.9% and increases throughput by 1,119–3,385 tokens/s across all three architectures and both GPU types. These gains are robust and reproducible, demonstrating that the acceleration is not specific to a particular model family or hardware platform.

G.3.3. SCALING ABILITY OF FOLDING TECHNOLOGY

Batch Size To assess scalability with respect to batch size, we conduct additional experiments on BERT using a single NVIDIA V100-32GB GPU with a fixed sequence length of 256. Batch sizes are varied from 4 to 128 (powers of two). The same measurement protocol is used: 50 warm-up inferences, followed by 50 measured inferences, repeated 5 times, with results averaged.

As shown in Table 15 and Table 16, the proposed method maintains stable and consistent performance gains across the full batch-size range. Latency reduction ranges from 2.58% to 6.45%, while the absolute throughput gain increases progressively with batch size, reaching +4,435 tokens/s at batch size 128. These results confirm that the acceleration mechanism scales effectively with batch size and does not degrade under higher memory or compute intensity.

G.3.4. SCALING WITH SEQUENCE LENGTH

Sequence Length To evaluate how the gains evolve with sequence length, we conduct experiments on BERT, GPT-2, and OPT using a single NVIDIA A100-40GB GPU with a fixed batch size of 4. The input/output sequence length is varied from

Table 15. Average inference latency (seconds) of BERT-base on a single V100 GPU (sequence length 256) across varying batch sizes. Results are averaged over 5 runs \times 50 measured inferences after 50 warm-up steps.

Batch Size	Original Inference Time (s)	New Inference Time (s)	Acceleration (%)
4	0.0201	0.0193	3.99
8	0.0360	0.0347	3.64
16	0.0693	0.0675	2.58
32	0.1339	0.1269	5.25
64	0.2557	0.2418	5.45
128	0.5092	0.4763	6.45

Table 16. Average inference throughput (tokens/second) of BERT-base on a single V100 GPU (sequence length 256) across varying batch sizes. Results are averaged over 5 runs, each with 50 measured inferences after 50 warm-up steps.

Batch Size	Original Throughput (tokens/s)	New Throughput (tokens/s)	Δ (tokens/s)
4	51029.1	53147.9	+2118.8
8	56920.5	59071.2	+2150.7
16	59148.0	60715.7	+1567.6
32	61185.0	64577.2	+3392.1
64	64072.1	67761.8	+3689.8
128	64357.4	68792.8	+4435.4

64 to 16,384 tokens. All measurements follow the same protocol: 50 warm-up inferences, 50 measured inferences, repeated 5 times, with results averaged across runs.

Table 17. Average inference throughput (tokens/second) of BERT-base on a single A100 GPU (batch size 4) across increasing sequence lengths.

Seq Length	Origin Throughput (tokens/s)	New Throughput (tokens/s)	Δ (tokens/s)
64	33464.1	34133.3	+669.3
256	67590.8	72572.6	+4981.9
1024	69072.5	77283.0	+8210.5
4096	46579.5	57115.6	+10536.1
16384	19349.4	25782.3	+6432.9

As shown in Table 17, Table 18, and Table 19, the proposed folding technique exhibits strong positive scaling with sequence length. On BERT, the absolute throughput improvement grows from +669 tokens/s at sequence length 64 to +10,536 tokens/s at 4096, and remains substantial (+6,433 tokens/s) even at 16,384 tokens. Correspondingly, the relative speedup also increases with sequence length, rising from 1.96% at 64 tokens to 24.95% at 16,384 tokens.

These results show that our method becomes increasingly effective as sequences grow longer, making it particularly valuable for modern long-context applications such as document-level reasoning, code generation, and retrieval-augmented systems. In contrast, as shown in Table 15 and Table 16, the acceleration remains relatively stable across batch sizes at fixed sequence length, confirming complementary scaling behavior along the batch and sequence dimensions.

Model Size To examine robustness across substantially different model scales, we further evaluate GPT-J-6B (Wang & Komatsuzaki, 2021), a 6-billion-parameter decoder-only Transformer that is approximately $48\times$ larger than GPT-2 (124M parameters) and $17\times$ larger than BERT (340M parameters) in non-embedding parameter count. All experiments are conducted on a single NVIDIA A100-40GB GPU following the same measurement protocol as above.

Table 20 and Table 21 report inference latency and throughput for representative (batch size, sequence length) configurations. Even on this substantially larger model, our method continues to deliver consistent and meaningful speedup. Relative latency reduction ranges from 4.2% to 7.7% across all in-memory configurations. The gains increase with sequence length, following

Table 18. Absolute throughput improvement (tokens/second) achieved by the proposed method across sequence lengths (batch size 4, single A100 GPU).

Model	64	256	1024	4096	16384
BERT	+669.3	+4981.9	+8210.5	+10536.1	+6432.9
GPT-2	+1193.0	+4890.3	+6235.8	+8806.8	+8182.2
OPT	+4697.6	+3639.8	+4145.0	+5558.0	+4630.1

Table 19. Relative inference speedup achieved by the proposed method across sequence lengths (batch size 4, single A100 GPU).

Model	64	256	1024	4096	16384
BERT	1.96%	6.86%	10.62%	18.45%	24.95%
GPT-2	4.23%	6.65%	8.50%	13.88%	21.47%
OPT	14.13%	5.09%	5.17%	8.04%	11.51%

Table 20. Average inference latency of GPT-J-6B on a single A100-40GB GPU. The proposed method achieves 4.2%–7.7% latency reduction, with larger gains at longer sequences. OOM denotes out-of-memory.

Batch Size	Seq Length	Original Inference Time (s)	New Inference Time (s)	Acceleration (%)
4	64	0.2030	0.1931	4.89
4	256	0.7840	0.7453	4.94
4	1024	3.0976	2.8637	7.55
8	64	0.4187	0.4010	4.22
8	256	1.5709	1.4666	6.64
8	1024	6.2038	5.7415	7.45
16	64	0.7793	0.7409	4.92
16	256	2.9893	2.7601	7.67
16	1024	OOM	OOM	\

Table 21. Inference throughput (tokens/second) of GPT-J-6B under the same settings as Table 20. The proposed method consistently improves throughput by 53–114 tokens/s, with the largest absolute gains appearing at longer sequences.

Batch Size	Seq Length	Original Throughput (tokens/s)	New Throughput (tokens/s)	Δ
4	64	1260.9	1325.7	+64.8
4	256	1306.1	1374.0	+67.9
4	1024	1322.3	1430.3	+108.0
8	64	1223.0	1276.8	+53.8
8	256	1303.8	1396.4	+92.7
8	1024	1320.5	1426.8	+106.3
16	64	1314.1	1382.0	+68.0
16	256	1370.2	1484.0	+113.8
16	1024	OOM	OOM	\

the same “longer-is-better” trend observed on smaller models. Absolute throughput improvement reaches +108–114 tokens/s at sequence length 1024, which becomes substantial when amortized over large-scale generation workloads.

These results confirm that the acceleration mechanism remains effective when moving from hundred-million-scale models (GPT-2, BERT, OPT) to multi-billion-parameter models, with no clear sign of diminishing returns.

Table 22. Relative speedup comparison between GPT-2 (124M) and GPT-J-6B (6B) on identical hardware and settings (single A100-40GB GPU, batch size 4).

Model	Parameters	SeqLen=256 Speedup	SeqLen=1024 Speedup
GPT-2	124M	6.65%	8.50%
GPT-J	6B	4.94%	7.55%

Moreover, comparing GPT-2 and GPT-J shows that even when the parameter count increases by nearly 50×, the relative speedup remains comparable (roughly 5%–8%), demonstrating strong scalability with model size.

H. Empirical Experiments

Consider a sample \mathbf{x} , with dimension d . We have the equation of LN and RMSNorm as follows:

$$\text{LN}(\mathbf{x}) = \frac{\mathbf{x} - \mu}{\sqrt{\sigma^2 + \epsilon}}, \text{ where } \mu = \frac{1}{d} \sum_{i=1}^d x_i \text{ and } \frac{1}{d} \sum_{i=1}^d (x_i - \mu)^2. \tag{54}$$

$$\text{RMS}(\mathbf{x}) = \frac{\mathbf{x}}{\sqrt{\sigma_{rms}^2 + \epsilon}}, \text{ where } \sigma_{rms}^2 = \frac{1}{d} \sum_{i=1}^d x_i^2. \tag{55}$$

It is worth mentioning that we compare custom-PyTorch module implementations of RMSNorm and LayerNorm (implemented according to Eqn.54 and Eqn.55), both without CUDA kernels to isolate algorithmic speedup.

H.1. Text Classification Task

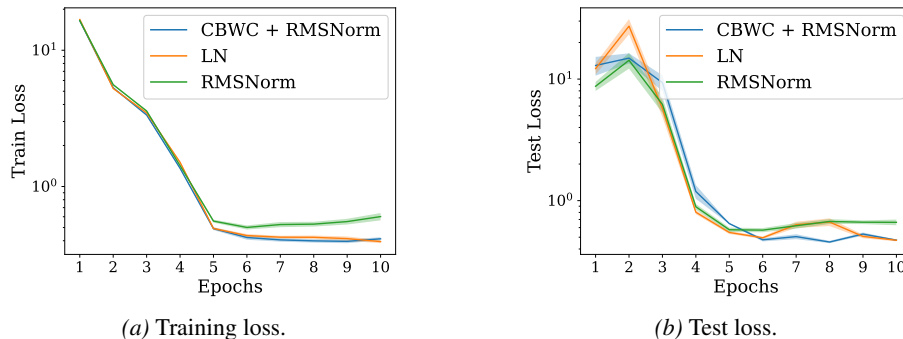


Figure 18. Performance of transformer models for text classification task of Transformer on the AG News dataset. The results are averaged over 5 random seeds with shaded regions indicating standard deviation

The experiment is conducted on a 3090Ti. The average results are reported in Table 23 and Figure 18. The best results are highlighted in bold, and the worst are shown in gray.

Table 23. Performance of Transformer on text classification.

Method	Test Loss	Test Acc (%)
LN	0.472 ± 0.010	85.21 ± 0.35
RMS	0.663 ± 0.037	76.57 ± 1.77
CBWC+RMS	0.473 ± 0.007	85.12 ± 0.23

H.2. Image Classification

For the Imagenet100, we select 100 classes from Imagenet1k (Deng et al., 2009) according to the given classes in (Tian et al., 2019). We chose SWIN-T for this experiment and trained on a single 3090. We apply the AdamW optimizer with a learning rate of 10^{-4} and a batch size of 128. Here we list the top 1 and top 5 accuracy and loss for both test and training in Table 24. We have the best results in bold and the worst results in gray.

Table 24. Average training results (mean \pm std) under 3 random seeds for SWIN on ImageNet100.

Model	TrainAcc@1 (%)	TrainAcc@5 (%)	TrainLoss
LN	99.397 \pm 0.003	99.919 \pm 0.010	0.0254 \pm 0.0002
RMS	99.376 \pm 0.004	99.913 \pm 0.001	0.0258 \pm 0.0004
CBWC+RMS	99.382 \pm 0.032	99.922 \pm 0.005	0.0257 \pm 0.0009

We use `time.time()` to trace the time usage. This strategy is consistent with practices in prior efficiency-focused works (Jiang et al., 2023), where authors also compared unoptimized module versions when no fast official RMSNorm existed.

Moreover, to verify the training stability of our method, we applied different learning rates on the models. We trained 70 epochs for each group.

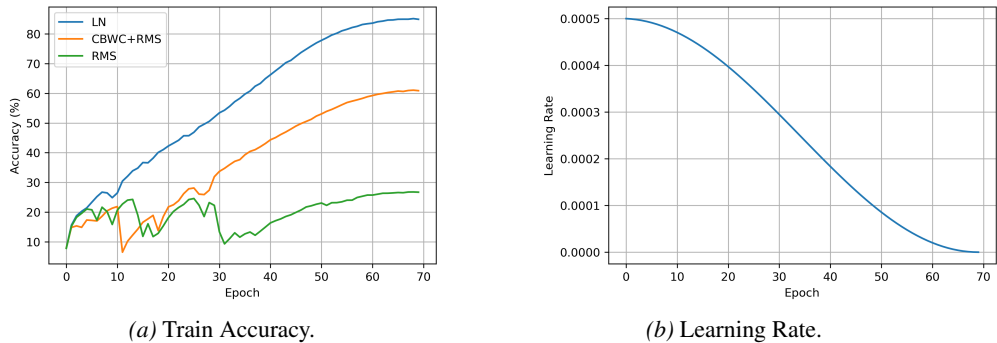


Figure 19. Train accuracy of three models and learning rate setting of SWIN transformer on Imagenet100 under high learning rate setting.

Under a higher learning rate (10^{-3}), CBWC+RMS performs between the LN and RMSNorm variants. As shown in Figure 19, with the decline of the learning rate, our method shows better stability as it can adapt to a higher learning rate. We also notice a more inclined accuracy curve, which is the evidence of faster convergence.

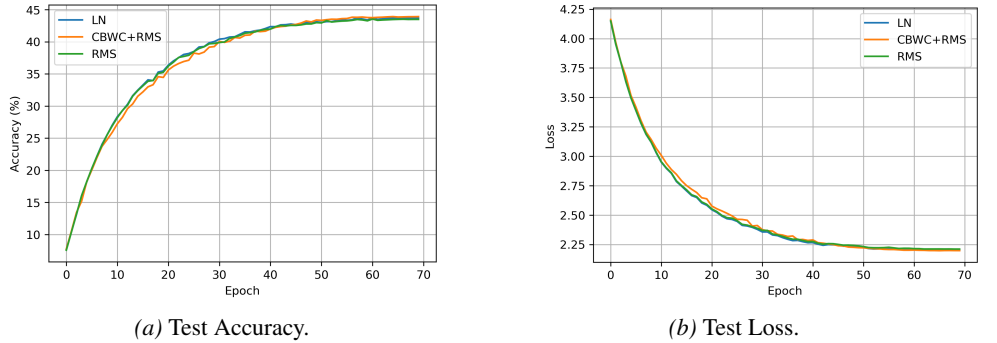


Figure 20. Performance of the three models in SWIN transformer on Imagenet100 under small learning rate.

Under a smaller learning rate (10^{-5}), the accuracy and loss of LN variant and RMSNorm are almost the same, while our method has different performance. Our method shows slightly better generalization performance than the variants using only RMSNorm or LN, with slightly higher test accuracy and lower test loss (as shown in Figure 20a and Figure 20b).

H.3. Text Generation

We also conduct a text generation experiment using GPT-3, and report the results in Table 25.

Table 25. Performance of GPT-3 on WikiText-103.

Method	Train Loss	Train PPL	Test Loss	Test PPL
LN	6.24	513	6.0598	428.30
RMS	6.32	557	6.1311	459.94
CBWC+RMS	6.18	484	6.0144	409.28

H.4. Verification Experiment for Fine-tuning on Pre-trained Model

H.4.1. EXPERIMENT SETTING FOR MLP

We verify that the CBWC+RMSNorm and original LN training scheme are identical in engineering by the following experiment.

We perform a classification task on CIFAR-10 (Krizhevsky, 2009). The MLPs have a depth of 6 and a width of 256. We train the models for 40 epochs with a learning rate of 0.01 and a batch size of 256, using a constant seed. The proxy parameter W_A and the original weight matrix W_B differ by less than 10^{-5} . As shown in Figure 21, the difference between the two parameter sets is negligible and can be attributed to numerical error. We therefore conclude that the two models follow indistinguishable optimization processes and can be inter-converted at any point during training without affecting the outcome.

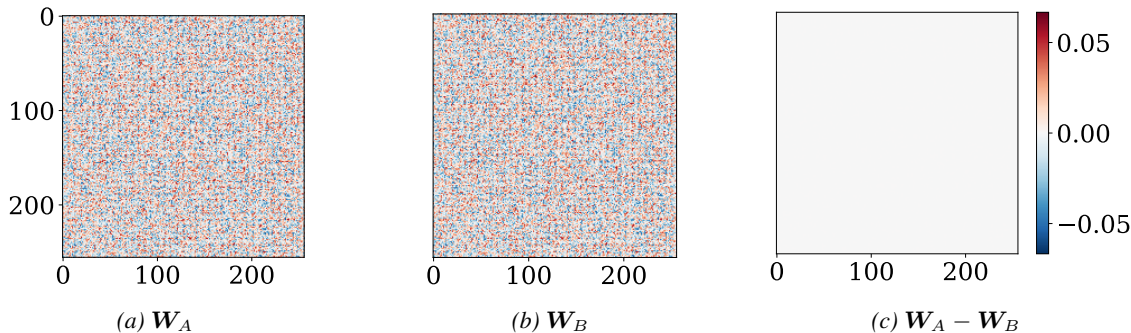


Figure 21. Comparison of W_A and W_B .

H.4.2. EXPERIMENT SETTING FOR TRANSFORMER

We pre-train the model with a learning rate of 5×10^{-4} and an effective batch size of 128 (batch size is 2 and gradient accumulation is 64). For fine-tuning, we have a learning rate of 5×10^{-5} and an effective batch size of 16 (batch size is 2 and gradient accumulation is 8).

I. Open-source Code

To facilitate verification and further experimentation, we release the complete open-source implementation, including the fully automatic folding tool and optimized RMSNorm kernels: <https://github.com/BobYue-01/Enjoy-LN>.